New Strategy for Band Gap Tuning of ZnS Nanostructures for Photocatalytic and Solar Cell Application

A dissertation submitted to the Department of Chemistry, Quaid-i-Azam University, Islamabad, in partial fulfillment of requirement for the degree of

Master of Philosophy

In

Inorganic/Analytical Chemistry

By

Abdul Ghafoor

Department of Chemistry
Quaid-i-Azam University
Islamabad

2017

New Strategy for Band Gap Tuning of ZnS Nanostructures for Photocatalytic and Solar Cell Application

A dissertation submitted to the Department of Chemistry, Quaid-i-Azam University, Islamabad, in partial fulfillment of requirement for the degree of

Master of Philosophy

In

Inorganic/Analytical Chemistry

By

Abdul Ghafoor

Department of Chemistry

Quaid-i-Azam University

Islamabad

2017

DECLARATION

This is to certify that this dissertation entitled **"New Strategy for Band Gap Tuning of ZnS Nanostructures for Photocatalytic and Solar Cell Application"** submitted by **Mr. Abdul Ghafoor** is accepted in its present form by the Department of Chemistry, Quaid-i-Azam University, Islamabad, Pakistan, as satisfying the partial fulfillment for the degree of **Master of philosophy in Inorganic/Analytical Chemistry**.

External Examiner: _____

Supervisor: _____

Assistant Prof. Dr. Zia-Ur-Rehman

Department of Chemistry
Quaid-i-Azam University
Islamabad

Head of Section: _____

Prof. Dr. Amin Badshah

Department of Chemistry
Quaid-i-Azam University
Islamabad

Chairman: _____

Prof. Dr. Muhammad Siddiq

Department of Chemistry
Quaid-i-Azam University
Islamabad

IN THE NAME OF ALLAH, THE MOST GRACIOUS, THE MOST MERCIFUL

DEDICATED TO MY LOVING PARENTS

Contents

List of figures

List of Tables

List of Schemes

Acknowledgement

First of all I am grateful to ALMIGHTY ALLAH and the Holy Prophet Muhammad (SAW), for every good thing which I have in my life.

My gratitude is for my supervisor Assistant Prof. Dr. Zia-Ur-Rehman for his guidance, valuable suggestions and encouragements during my M.Phil research work.

I am indebted to my most respected father and I am thankful to Almighty Allah that my beloved mother prays for my success today and huge contribution in my achievements is because of her prayers. I am thankful to my family members my sisters and brothers (Fazal Ghafoor, Rahmat Ghafoor and Afzal Ghafoor) especially for their continuous support and encouragement.

I would like to extend my wholehearted thanks to Prof. Dr. Muhammad Siddiq (Chairman of Department) and Prof. Dr. Amin Badshah (Head of Inorganic/Analytical Section), and all my honorable teachers for their efforts and help.

A deep sense of gratitude to Mr. Niaz Ali for SEM, TEM and EDS and Prof. Dr. Zareen Akhter and her research group for UV-Vis DRS.

I am thankful to all my lab fellows and friends for their support during my research work.

I am thankful to the technical staff at the Department of Chemistry, Quaid-i-Azam University Islamabad.

Abdul Ghafoor

Abstract

The controlled synthesis of pure ZnS and $Zn_{1-x}Cd_xS$ nanostructures has been achieved using a new strategy which involves three facile steps. First, Sodium salt of dimethyldithiocarbamate $(CH_3)_2NS_2Na$ was prepared by a reported method from dimethylamine, carbon disulfide and sodium hydroxide. Second, single source precursors $Zn_{1-x}Cd_x$-$(DMDTC)_2$ (x= 0, 0.2, 0.3, 0.5, 0.6) were prepared via direct precipitation reaction of stoichiometric amount of zinc nitrate, cadmium nitrate and sodium dimethyldithiocarbamate in methanol at room temperature. Third, hexagonal phase ZnS and $Zn_{1-x}Cd_xS$ nanostructures (x= 0.2, 0.3, 0.5, 0.6) with different aspect ratio were synthesized by simple reflux method via thermal decomposition of self-prepared precursors in the presence of octylamine at 120 ^oC. The obtained products were characterized by PXRD, UV-Vis DRS, SEM, TEM and EDS analysis. It was noticed that optical bandgap energy was shifted continuously to the visible region with increase of cadmium incorporation. Their photocatalytic activity was investigated for photodegradation of methylene blue dye and highest degradation rate with rate constant of 4.30×10^{-2} min^{-1} was observed for $Zn_{0.4}Cd_{0.6}S$ as compared to 7.60×10^{-3} min^{-1} for pure ZnS. Thus, they are promising material to be used for photocatalytic and solar cell application.

Chapter 01 Introduction

1.1 Introduction to Nanostructured Materials

Those materials which have dimensions in between 1-100 nm are termed as nanostructured materials. These nanostructured material have got much more attention because of certain exceptional properties [1]. For example these materials have large surface area due to their small size, large surface to volume ratio and have high adsorption capacity and thus show higher capability especially in field of catalysis. Nanostructured have not only attracted higher attention in field of research but gradually intruded in to every day need and requirements [2-4]. According to the well-known statement of Richard Feynman in 1959 that there is various opportunities based on the principle of physics, the possibility of designing materials atom by atom can miniaturize as the chemist says and so design the substance for vast application. This consideration come true in less than half a century because of regular struggles and fruitful contribution from the scientific community across the globe [5].

1.2 Introduction to ZnS Nanostructures

Zinc sulfide is one of the inorganic metal chalcogenide semiconductor [6]. ZnS exhibit remarkable fundamental properties and is a promising material for diverse application like LEDs, optical detector, gas sensor, window material, solar cell and photocatalyst etc. Like ZnO, a most widely studied semiconductor, ZnS have also atomic structure and chemical properties comparable to ZnO. There are certain unique properties and advantages of ZnS in comparison with ZnO namely larger band gap of 3.72-3.77 eV as compared to ZnO which is 3.4 eV. Due to this reason it is a promising material to be used in visible–blind ultraviolet light based sensor and photodetector. Similarly, ZnS is also a suitable material for electroluminescence [7].

1.3 Allotropic Forms of ZnS

Zinc blend and wurtzite are the two different allotropic forms of ZnS in which it commonly occur. Zinc blend have cubic geometry while wurtzite possess hexagonal symmetry. The

cubic form is the stable low-temperature phase, while the hexagonal is the high-temperature polymorph which forms at around 1296 K. **Figure 1.1** shows various sights for comparison in these structures. The dihedral conformation can best explain their difference. Zinc blind form have sulfur and zinc atom that are coordinated tetrahedrally in ABCABC stacking pattern with ccp packing. On other hand wurtzite form have the same coordination having ABAB stacking pattern with hcp packing.

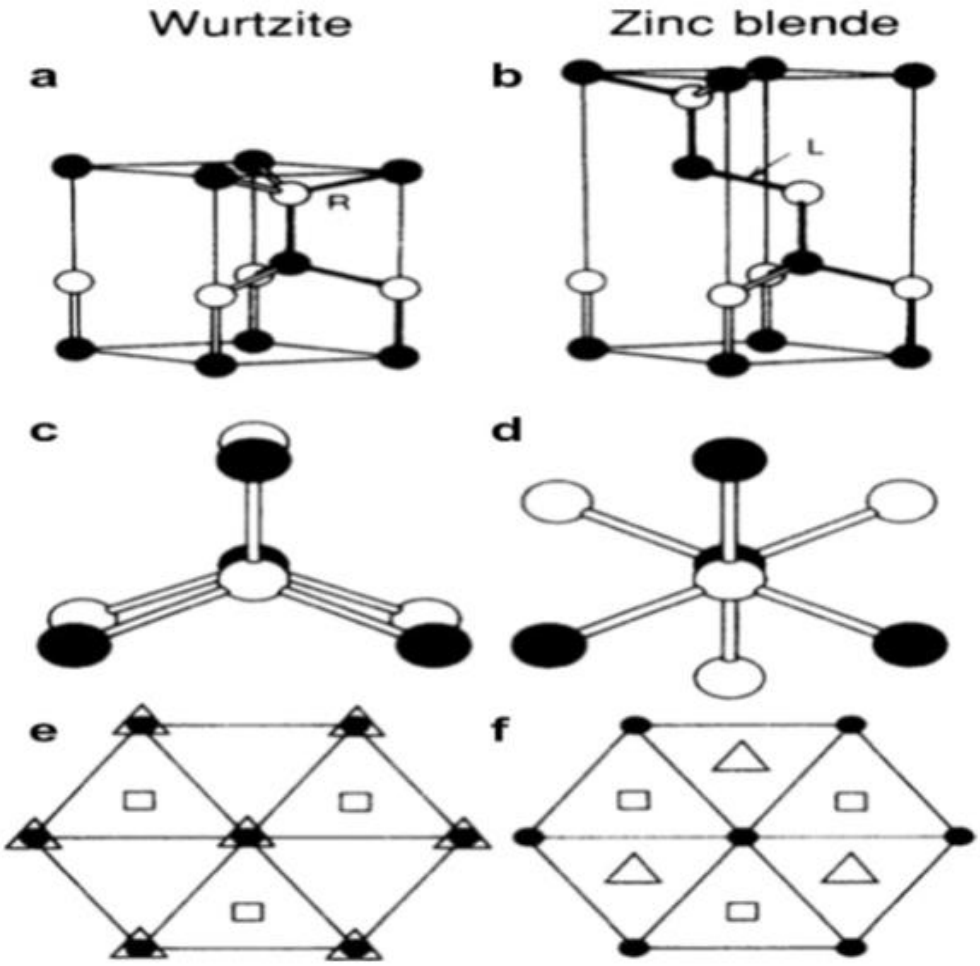

Figure 1.1 Models showing the difference between wurtzite and zinc blende crystal structures. (a and b) Show handedness of the fourth interatomic bond along the right (R) for wurtzite and along the left (L) for zinc blende. (c and d) The respective eclipsed and staggered dihedral conformations. (e and f) Show atomic arrangement along the close packing axis [8]

1.4 Tuning the Band Gap of ZnS Nanostructure

The important parameters which decide the use of semiconductor nanostructure for a particular application is its morphology and band gap energy. Band gap energy of the nanostructure can be adjusted for a particular application with changing the size of the nanostructures which is related to quantum confinement effect. But decrease in size below 2 nm results in problem of instability which hinders the wide application of the nanostructures in various fields.

However, an effective approach through which optical properties like band gap along with electrical, magnetic and structural properties can be tuned for desired application is the change in the composition of nanostructured materials [9-14].

1.5 Various Approaches of Compositional Variation in ZnS Nanostructure for Tuning their Properties

1.5.1 Modifying With Narrow Band Gap Semiconductor

In recent times, composite nanostructures have attracted much more attention as new optical and electrical properties appears due to the combination of two different semiconductor nanostructures [15, 16]. Generally, composite materials with nanostructures can be prepared by mixing different nanostructures with a micelles like chemical that act as processable medium. Different nanocomposite with nanostructure like quantum dots quantum well of tunable band gap have been synthesized by inserting or sandwiching a material of low band gap between the layers of material having higher band gap like, ZnS/PbS/ZnS [17], CdS/HgS/CdS [18], ZnS/CdSe/ZnS [19] nanocomposites. These investigations shows that different electrical and optical properties have been appeared.

ZnS/CdS/ZnS composite with nanostructures have been successfully prepared by using chemical method at a temperature of 80 ^{o}C. The UV-Visible spectra of these synthesized nanocomposite with CdS of different thickness being is shown in **Figure 1.2**. A continuous red shift is observed in absorption edge as a function of CdS thickness. This bathochromic shift may be attributed to the outflow of electronic wave function into the CdS layer from ZnS core.

\

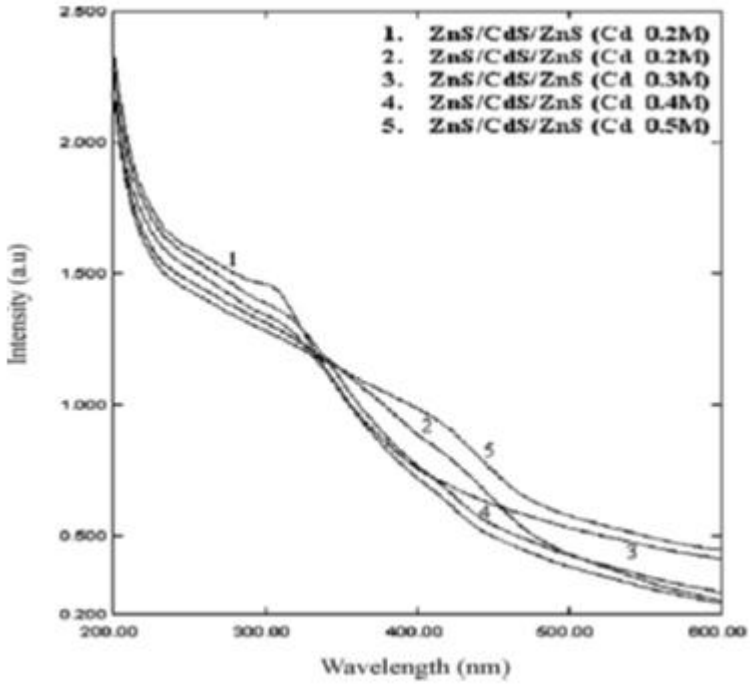

Figure 1.2 UV-vis spectra of ZnS/CdS/ZnS nanocomposites with different thickness of CdS [20]

1.5.2 Doping with Non Metals

A novel C,N codoped ZnS nanoporous, nanostructures was synthesized by thermal decomposition method at various decomposition temperature using zinc isothiocyanate as a source for Zn, C and N. There was no templet or catalyst used during their synthesis. The synthesized nanoporous nanostructure exhibited visible light response.

Figure 1.3 shows the UV-Vis DRS spectra of the commercial pure ZnS as well as that of synthesized C,N codoped ZnS at various temperature. A clear red shift in to the visible region is being observed in case C,N codoped ZnS relative to the commercial pure ZnS. This bathochromic shift may be attributed to the formation of new energy levels within the ZnS band structure upon C,N codoping. This study gives us insight that photoabsorption capability of ZnS can be extended in to the visible region also with nonmetal codoping like carbon and nitrogen.

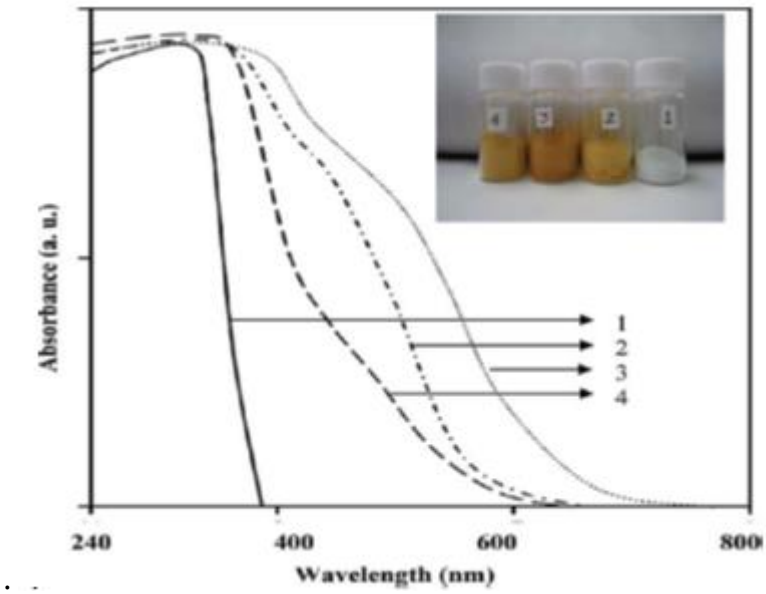

Figure 1.3 Diffuse reflectance spectra of (1) pure commercial ZnS, (2) ZnS prepared at 300 °C, (3) ZnS prepared at 400 °C, and (4) ZnS prepared at 500 °C; the inset picture shows the corresponding catalysts[21]

1.5.3 Introducing Intrinsic Vacancies Defects in ZnS Nanocrystal

The band gap of ZnS can also be tuned to the visible region through formation of vacancies in the ZnS nanocrystal. Vacancy is a type of intrinsic effect in which an atom with in a crystal is removed. Vacancy defect can be obtained easily only in the case of quasi-two-dimensional substances because of an easy escape of the exposed atom on the surface from their lattice and thus can change physical as well as the chemical properties. It has been proposed through theoretical studies that introduction of S vacancy in the ZnS crystal lattice is easy compared to the Zn vacancy and incorporation of S vacancy can decrease its band gap to the visible region.

ZnS with controlled S vacancy have been synthesized with help of hydrothermal method reacting Zn and S powder with NaOH solution of higher concentration in the presence of $NaBH_4$ which act as reducing agent. As a result of S vacancy in the ZnS, the absorption spectra extended to the visible region competently. To check the synthesized ZnS with S vacancy for photocatalytic activity, it was used as a photocatalyst for hydrogen production in the presence of visible light where the hydrogen produced was determined by gas chromatograph. The results showed the photocatalytic activity of the synthesized ZnS

increases with increase in S vacancy and similarly the S vacancies increases with increase in concentration of $NaBH_4$. This gives the conclusion that amount of S vacancy can be controlled with concentration of $NaBH_4$. Their DFT calculation showed that extra energy levels are appeared within the band gap of ZnS that are responsible absorption in the visible region.

Figure 1.4 shows the UV-Vis DRS spectra of the commercial ZnS (ref) as well as of the synthesized ZnS with different concentration of sodium borohydride. The colour of the synthesized sample are also shown in the figure as inset. From the figure it is clear that reference ZnS does not show absorption in the visible region. While the synthesized ZnS without addition of sodium borohydride shows absorption in the visible region but in this case the visible light absorption cannot be controlled and the photocatalytic activity of this sample was also insignificant. The figure clearly shows that absorption capacity of the samples extend to the visible region with increase of sodium borohydride.

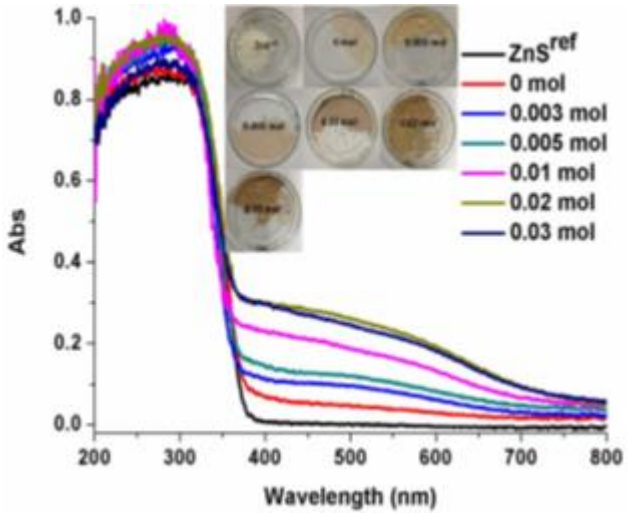

Figure 1.4 UV-Vis diffuse reflectance spectra of ZnS synthesized using 0– 0.03 mol of $NaBH_4$ [22]

1.5.4 Doping with Metals

Like other approaches, the band gap of the ZnS nanostructures can also be tuned by doping with metal ions which is a most widely used approach because ZnS shows the properties like low toxicity and chemical as well as physical stability which make it a promising host material. Different metal ions have doped successfully in the ZnS nanocrystal resulting in unique physical and chemical properties [23-25]. For instance, different metal ions like Mn^{2+}, Cu^{+}, Pb^{2+}, Ag^{+}, and Eu^{2+} have been incorporated in ZnS nanocrystal successfully which exhibit different optical properties [26-30]. This is because in doped ZnS nanostructure the impurity ions act as recombination center for the photoexcited charge carriers which leads to different optical properties like photoluminescence and electroluminescence in the different regions of the UV-Visible spectrum [31]. Nevertheless, the band gap of ZnS nanostructure have been found to be extended into the visible region with doping of metal ions , although its band gap may also increase which in turn depend on nature and concentration of impurity ion according to Burstein-Moss shift [25].

ZnS microspheres with a series of Mn-doping concentration were prepared by a facile solvothermal route. The light absorption characteristics of the prepared samples are shown by UV–visible diffuse reflectance spectra (DRS). Pure ZnS only exhibits absorption in the UV region and the absorption edge is at about 375 nm, while the Mn-doped ZnS samples display long-tailed absorption in the visible light region and the absorption exhibit bathochromic shift with increase of the Mn content. The color of the samples gradually deepens from white to yellow as seen in the inset picture. ZnS is known as a typical direct bandgap semiconductor and a sharp increase in the absorbance is shown by it which is due to its intrinsic transitions as it is coincident well with the shape of spectrogram.

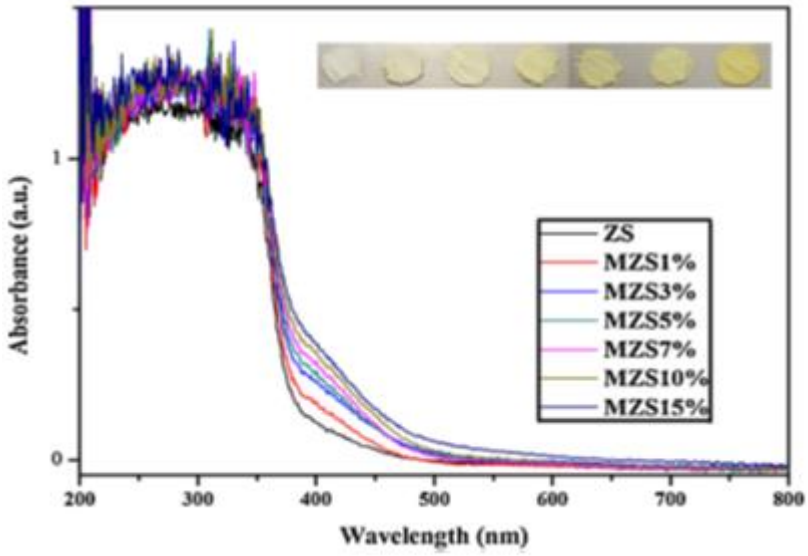

Figure 1.5 UV–vis diffuse reflectance spectra of Mn-doped ZnS [32]

1.5.5 Making ZnS Based Solid Solution

The band gap of ZnS can also be narrowed by making ZnS based solid solution with incorporation of other metal ion like Cd^{2+} ion to form ternary sulfides [33-41]. $Zn_{1-x}Cd_xS$ ternary sulfide nanostructures have a cheerful scene for various applications. Because it is almost understood that when solid solutions of wide band gap semiconductor are prepared with a semiconductor of narrow band gap, the band gap of the solid solution can be controlled and material of desired band gap can achieved. ZnS is a wide band gap semiconductor with band gap energy roundabout (*E*g 3.67 eV) which lies in the UV region; when introducing Cd, these compounds can form $Zn_{1-x}Cd_xS$ solid solutions with a narrow band gap lying in the visible region. This can be used as visible light responsive photocatalyst. This is very effective approach for band gap narrowing of ZnS as well as for synthesizing visible light stable with higher photocatalytic efficiency photocatalyst then common CdS [42]. Our study is also concerned with band gap tuning of ZnS nanostructures in order to extend its absorption capability to the visible region for photocatalytic and solar cell application by incorporating Cd^{2+} and making $Zn_{1-x}Cd_xS$ solid solution.

1.6 Introduction to $Zn_{1-x}Cd_xS$

$Zn_xCd_{1-x}S$, a kind of ternary sulfides which exhibit fine and tunable absorption in the visible region of solar spectrum and outstanding electrical conductibility, due to this reason, these ternary sulfides are well known to be a suitable candidates for photocatalytsis [43, 44]. $Zn_xCd_{1-x}S$ exhibit photocatalytic properties better then ZnS and CdS and have band gap that can be varied in a controlled manner with varying Zn^{2+}/Cd^{2+} atomic ratio in their solid solution.

1.7 Importance of $Zn_{1-x}Cd_xS$

Recently the field of photocatalytic oxidation has got greater attention for designing best photocatalyst with special emphasis in TiO_2 to be used in a verity of snags of environment like water and air treatment [45]. TiO_2 is the most widely studied and applied photocatalyst but the main limitation is that it needs UV light due to their larger band gap for their application as a photocatalyst. So its application in visible light is not fruitful.

Development of visible light driven photocatalyst is one of the main research topic that researcher has specially focused on it, in order to utilize or take advantage of the solar light resources more effectively as visible light constitutes a larger portion then UV light in solar irradiation [46]. Metal chalcogenide because of suitable band edge position and band gap energy, have provoked higher attention in photocatalysis. Among hundreds of candidates that comprising inorganic compounds and semiconductors, cadmium sulfide and zinc sulfide have attracted much interest because of their fascinating optical and electronic properties (quantum size effect) as well as their latent applications in optoelectronic devices and photovoltaic cells [46-48].

Cadmium sulfides and zinc sulfides are famous and widely used narrow and wide bandgap semiconductors of group II–VI having band gaps energy round about 2.4 and 3.5 eV, respectively [49]. Cadmium sulfide is a most favorable photocatalyst to be used for various photocatalytic activities, like photocatalytic water splitting and organic pollutants (dyes) photodegradation because of its band gap energy that lies in the visible region and suitable conduction and valence band positions [50]. Similarly, zinc sulfide is also a fascinating photocatalyst to be used like cadmium sulfide in various photocatalytic application due to exhibiting high converging efficiency which may be attributed to their relative negative

reduction potential of the conduction band, however, due to its large band gap it can be used as photocatalyst only in the presence of ultraviolet light [51]. Cadmium sulfide although is a better photocatalyst due to its suitable band gap but there are some limitation related to its which hinder its versatile applications in photocatalysis like , the rapid recombination of charge carriers (electron and hole pairs) that are produced as interaction of light with photocatalyst and another limitation is photocorrosion which is the decomposition of cadmium sulfide as a result of irradiation for long time into sulfur or sulfate ion and cadmium ion [36, 52] on other hand zinc sulfide which is a less toxic as well as chemically and physically stable semiconductor can be used as a good material for the fabrication of ZnS based solid solution that can act as photocatalyst in visible light [52].

To solve these problems related both to CdS and ZnS, formation of $Zn_{1-x}Cd_xS$ solid solution may be regarded as a useful approach due their same mode of coordination [53]. Similarly, with varying Zn/Cd atomic ratios in the $Zn_{1-x}Cd_xS$ their structural properties (band gap and band edge position) and optical properties can be tuned for a particular application [52, 54]. That is why, formation of the $Zn_{1-x}Cd_xS$ solid solution is of immense technological importance.

1.8 Bandgap width and Band Edges Position with Zn/Cd ratio and its Relation with Photocatalytic Activity

Theoretically, the conduction band of $Zn_{1-x}Cd_xS$ is composed of the hybridized Cd 5s5p and Zn 4s4p orbitals while the valence band of $Zn_{1-x}Cd_xS$ is formed by the hybridized Cd 4d, Zn 3d and S 3p orbitals. When the Zn content is increased, the conduction band bottoms shift toward a more positive energy level and the valence band tops shift toward a more negative position. As a consequence, the optimum band gap and a suitable position of conduction of $Zn_{1-x}Cd_xS$ can be achieved by controlling the ratio of Zn and Cd [55]. Experimentally, $Zn_{1-x}Cd_xS$ with different shape and tunable band gap have been successfully synthesized and the enhanced photocatalytic activities have been attained compared with pure ZnS and CdS photocatalysts [56].

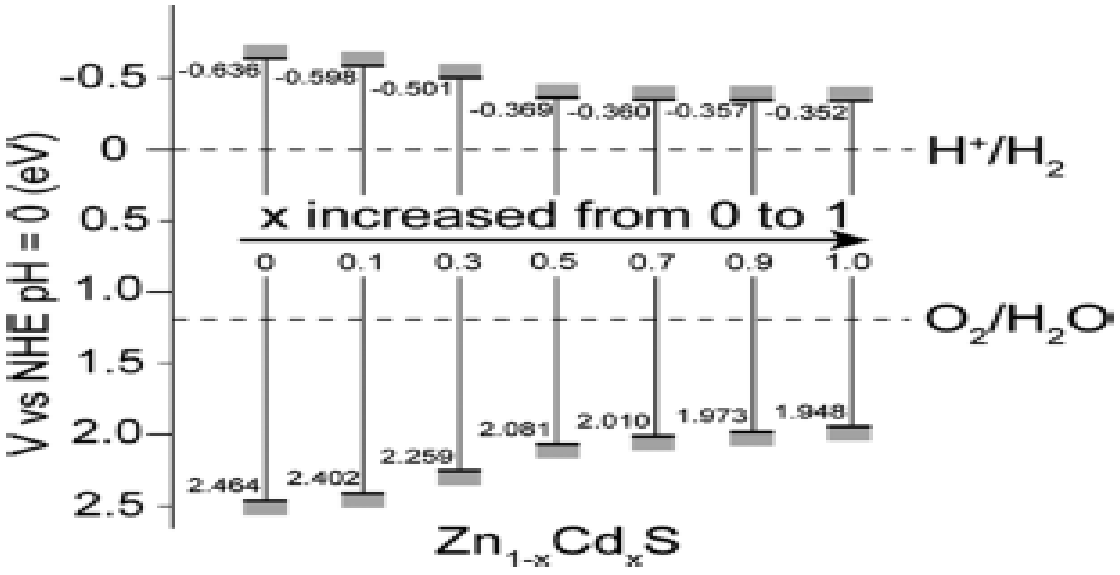

Figure 1.6 Conduction and valence band edge potentials of the $Zn_{1-x}Cd_xS$ (x = 0, 0.1, 0.3, 0.5, 0.7, 0.9, and 1.0) samples [47]

Figure 1.6 clearly shows that as the cadmium content increases in the $Zn_{1-x}Cd_xS$ ternary sulfides semiconductor solid solution the conduction band potential become more positive which reveals that $Zn_{1-x}Cd_xS$ with higher zinc content have better reduction power for water to produce hydrogen as compare to the $Zn_{1-x}Cd_xS$ with higher content of cadmium. But for photocatalysis higher content of zinc in the $Zn_{1-x}Cd_xS$ is not desirable because of band gap broadening. Usually, for better photocatalytic activity in the visible light, the band gap of suitable magnitude as well as the position of conduction and valence band potential are responsible. From the figure 1.6 taking the sample $Zn_{1-x}Cd_xS$ with x= 0.5 the band gap energy calculated is (2.45 eV) which shows narrower band gap as compared to (3.10 eV) that of ZnS. Similarly, the conduction band potential of the $Zn_{1-x}Cd_xS$ with x=0.5 is (-0.369 eV) which is relatively more negative to that of conduction band potential of CdS which is (-0.352 eV).So, an equilibrium between the band gap magnitude (which control light absorption capacity) and potential of conduction band energy level (that photocatalytic efficiency) in the $Zn_{1-x}Cd_xS$ may exhibit high photocatalytic efficiency as compare to pure ZnS and CdS [47].

1.9 Fabrication of $Zn_xCd_{1-x}S$ Solid Solution

Various synthetic method have been employed for the fabrication of $Zn_xCd_{1-x}S$ like hydrothermal method, cation exchange method, coprecipitation method, chemical bath deposition method and thermolysis method etc. Some of these conventional method have many limitations. For example in case of coprecipitation method, the stoichiometry in the final product are not maintain because of washing away of some metal ions during the synthesis [52]. Similarly in case of cation exchange method due to the larger ionic radius of Cd^{2+} (0.079 nm) as compare to Zn^{2+} (0.074 nm), the synthesis of $Zn_xCd_{1-x}S$ with controlled band gap is difficult while in case of hydrothermal method it takes much more time to obtain $Zn_xCd_{1-x}S$ with good crystallinity [57].

On other hand, the thermolysis method in which the precursor is subjected to a high temperature, commonly exhibit high formation rate of $Zn_xCd_{1-x}S$ solid solution in less time compared to other methods. $Zn_xCd_{1-x}S$ solid solution synthesized by thermolysis method also exhibit good crystallinity along with better photocatalytic activity [57]. Due to this reason we also synthesized the $Zn_xCd_{1-x}S$ solid solutions through thermal decomposition method using dithiocarbamate complexes as single source precursors.

1.10 Application of ZnS and ZnS Based Solid Solution Nanostructures

ZnS and $Zn_xCd_{1-x}S$ solid solutions have attracted higher attention especially in research field because of their potential application in various practical fields like in fabrication of gas sensors, solar cells and photocatalysts etc.

1.10.1 Gas Sensors

Like other met**a**l oxides ZnS may also be a good candidate for gas sensing because of its close fundamental physical and chemical properties with ZnO, including crystal structures, lattice constant and many other. However according to few reports [58] ZnS NWs suffer from the disadvantages of low response, slow rise and recovery speed which limits its practical application in detecting gas. So it is necessary to find some ways to improve the sensing properties of the ZnS nanostructures.

To improve the sensing performances, $Zn_xCd_{1-x}S$ NWs is considered to be a better alternative for the conductometric sensors. As Cd is more electronegative element then Zn

that is why CdS have shown very fast response speed to ethanol as compared to Low response of ZnS NWs.

Compositional combination between ZnS and CdS with different properties are expected to provide a new strategy to design high performance gas sensor. Solvothermal method was employed to synthesize a complete series of $Zn_xCd_{1-x}S$ nanowires which was further used for the fabrication of gas sensors. The novel sensors based on $Zn_xCd_{1-x}S$ NWs nanowires (especially when x = 0.4) exhibited better response for the ethanol as compare to the pure ZnS nanowires.

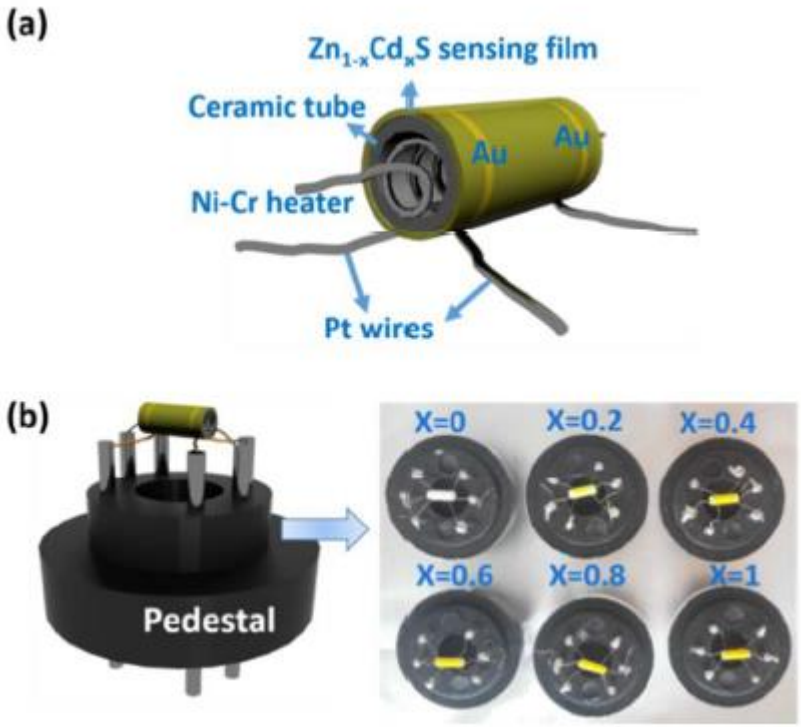

Figure 1.7 (a) Schematic image of the ceramic tube coated with the sensing material. (b) Schematic image of the device (left) and $Zn_xCd_{1-x}S$ sensors with different x value (right)[58]

1.10.1a Fabrication of Gas Sensor Device

The synthesized $Zn_xCd_{1-x}S$ NWs were uniformly mixed with water followed by sonication to get its paste which was further used for the fabrication of gas sensor device. A ceramic tube having a pairs of electrodes made of gold for the resistance measurement was used as

a substrate upon which the prepared paste was coated followed by insertion of a Ni-Cr wire as a heater and then welding the device on a pedestal. The Fabricated gas sensor devices were then allowed to age till 100 hours at 120 ^{o}C. **Figure 1.7** shows schematic structure $Zn_xCd_{1-x}S$ NWs based gas sensor device.

1.10.1b Gas Sensing Mechanism

Gas sensing mechanism can be explained by using a model that comprises the following three steps that are adsorption of gas, charge transfer process and desorption phenomenon. Current (*I)* to voltage (*V*) relation shows the ohmic behavior of gas sensors. The electrical conductivity and response of the sensor determine the resistance of the film sensor. When the oxygen form the surrounded air is adsorbed on the surface of film it is converted into oxygen ions (O_2^-, O^-,and O^{2-})by gaining electron from the conduction band of $Zn_xCd_{1-x}S$ NWs leading to the formation of depletion region at NWs surface and potential barrier at NWs-NWs junction as shown in the scheme 1. Due to the depletion layer then a modified potential is produce which confines the carrier into a smaller region as compare to the geometrical size of the NWs. At that time the oxygen-adsorption-induced potential energy barrier at the intersection blocked the electron flow. In the figure1.7* (a) E_{CB} is the conduction band minimum, E_{VB} is the valence band maximum, and φ is potential energy barrier at the intersection. Because of the formation of charge-space region NWs surface and potential barrier at NW-NW junction, the NW film show higher resistance in the presence of air. But as the ethanol gas which is reductive in nature is introduced, the charge transferring process restart. The ethanol molecules interact with adsorbed oxygen ions on the surface of NWs and then release the trapped electron back into the NWs resulting in thinner space-charge region and lower potential barrier decreasing the resistance of the NWs sensing film. Therefore, the process of the reaction in this work can be described as follows

$$C_2H_5OH\ (gas) \leftrightarrow C_2H_5OH\ (ads) \quad \textbf{(1)}$$

$$C_2H_5OH\ (ads) + 6O^-\ (ads) \rightarrow 2CO_2 + 3H_2O + 6e^- \quad \textbf{(2)}$$

When the sensors are exposed back to air after that, the electron capturing process starts, which increases the resistance of the sensing NWs film.

Mechanisms Responsible for the Resistance Changes in NW-Based Gas Sensors [a]

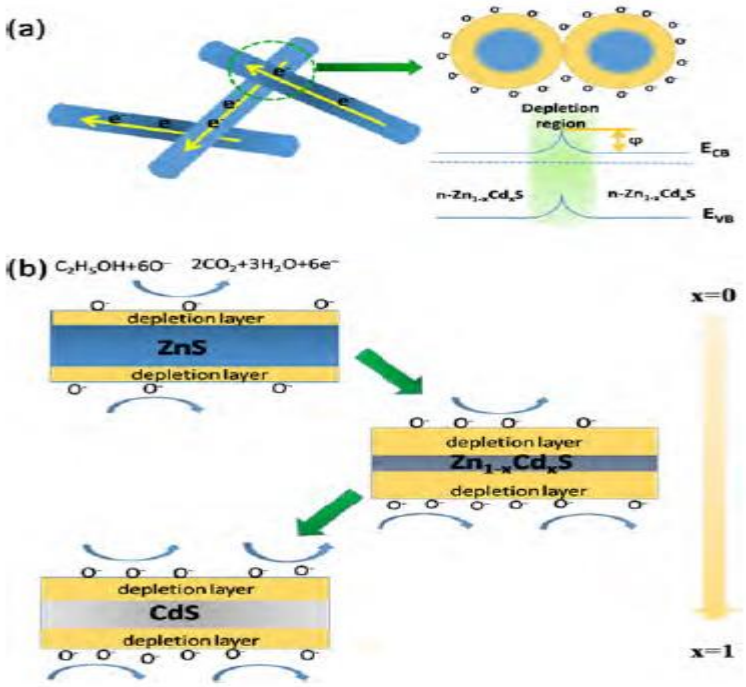

Figure 1.7* (a) Interfacial mechanisms for the crossed $Zn_xCd_{1-x}S$ NWs. (b) Dynamic equilibrium of two factors: the enhancement of the oxygen molecules absorption process and the increase of carrier intensity in the NWs in $Zn_xCd_{1-x}S$ NWs with the increase of x value[58]

1.10.2 Solar Cells

There are many sources of energy that are used for various purposes in the world but most of them are related with many problems, economical or environmental up to some extent. While the better, environmentally safe and renewable energy source is the conversion of solar energy to electrical energy. For this purpose solar cells are designed to take advantage of this huge source of energy and to overcome the world energy crisis.

Solar cells were conventionally built of silicon that is an inorganic material. Although these types of solar cells show high efficiency but very expensive materials and energy intensive processing technique was the main disadvantage. Hybrid and photo electrochemical (dye sensitized) solar cell are expected to be low cost alternative to these conventional silicon solar cells. However, Hybrid solar cells that comprise of inorganic as well as organic materials, hence combining the exceptional properties of inorganic semiconductor (like Zn_{1-}

$_x$Cd$_x$S etc.) and film forming properties of the conjugated polymers (like P3HT etc.). The use of organic material is advantageous because of low cost, easily processable and tailoring of their functionality by chemical synthesis and molecular design. Similarly, inorganic semiconductor that can be fabricated in nanostructured form offer an advantage of high absorption capacity because of their tunable optical properties that can be tuned with size and compositional variation in the nanostructures. Thus inorganic / organic hybrid concept is fascinating in recent years. There are various types of hybrid solar cells which comprises solid state dye sensitized solar cell, nanoparticle sensitized TiO_x solar cells, extremely thin absorber (ETA) solar cells and hybrid solar cells based on bulk heterojunction concept. We will discuss hybrid solar cell based on bulk heterojunction concept [59].

1.10.2a Hybrid Solar Cell Based on Bulk Heterojunction Concept

In this type of solar cell blend of semiconductor nanostructure with a conductive organic polymer as a photovoltaic layer is used. The basis of this is bulk heterojunction concept. Exciton created on photoexcitation are separated into free charge carriers at the interface between two semiconductor thin film such as conjugated polymer and metal sulfide nanostructures. Electron will be accepted by acceptor, a material with high electron affinity like ($Zn_{1-x}Cd_xS$ etc.) while the hole by the material with lower ionization potential, which act as electron donor usually the conducting organic polymer like P3HT etc. Bulk heterojunction hybrid cells have been designed in different semiconducting polymer containing CdSe, $CuInS_2$, CdS, PbS and $Cd_xZn_{1-x}S$ etc. However, $Cd_xZn_{1-x}S$ based hybrid solar cells is interesting in recent years [59].

1.10.2b Fabrication of $Zn_{1-x}Cd_xS$ Based Hybrid Solar Cells

For the fabrication of this type solar cells we need a substrate commonly ITO (indium tin oxide) coated glass which is a conducting glass, photoactive blend which consist of homogenous mixture of inorganic semiconductor nanostructure and ragio- regular P3HT (poly 3 hexyl thiophene) a conducting polymer and PEDOT-PSS (poly-ethylenedioxythiophene-poly) (styrene sulfonate). U.jabeen et al. fabricated this type of hybrid solar cells using ITO coated glass having resistivity 20 Ω/cm^2 as a substrate. In order to remove impurities these sheets were washed three times with water and acetone in an

ultrasonic bath. Then a thin layer (80 nm) of PEDOT-PSS (poly- ethylenedioxythiophene-poly) (styrene sulfonate) was spin coated on their surfaces at a rate of 4500 rpm for 45 s. The purpose of this layer was to facilitate the transport of holes towards anode. In the next step, the photoactive blend comprising of a homogeneous mixture of regio-regular P3HT (poly (3-hydroxy thiophene) and synthesized nanostructures ($Zn_{1-x}Cd_xS$) in the ratio of 30:70 was spin coated over the top of PEDOT-PSS at a rate of 1500 rpm for 20 s. This was immediately followed by another spin coating at a rate of 500 rpm for 20 sin order to evaporate the solvent and get a uniform layer. At last aluminum was deposited in the form of thin strips (80 nm) under high vacuum conditions using thermal evaporator. The devices were ready and annealed in an argon atmosphere at 90 ^oC for 15 min for improving morphology of the active blend [25].

1.10.2c $Zn_{1-x}Cd_xS$ and Efficiency of Solar Cell

The synthesized nanostructure $Cd_xZn_{1-x}S$ with (Cd content, X = 0.2, 0.3, 0.4, 0.5, 0.6 and 0.7) used in the fabrication of hybrid solar cells was subjected to current voltage measurement in order to study the effect of cadmium content on solar conversion efficiency of the devices in term of short circuit density $J_{sc.}$ The results shown in the **Figure 1.8** and tabulated in the **Table 1.1** depicts that Cd incorporated ZnS-P3HT used as photoactive blend exhibit high efficiency as compare to ZnS-P3HT.The results shows that efficiency of the fabricated devices increases with increasing cadmium content in $Cd_xZn_{1-x}S$. According to their work maximum efficiency have been observed in case when cadmium content x= 0.5wich is related to its lowest band gap among the whole series of the synthesized $Zn_{1-x}Cd_xS$ nanostructures and thus it shows 2.33 time higher efficiency as compare to the reference device have ZnS-P3HT as photoactive blend composition. Further than 0.5 M Cd content, the band gap can no more be decreased so efficiency of the device should also become constant but conflicting to expectations, the efficiency was decreased at 0.6 M and 0.7 M Cd content. This decrease could be associated to the presence of un-incorporated cadmium and the formation of CdS as an additional phase (25).

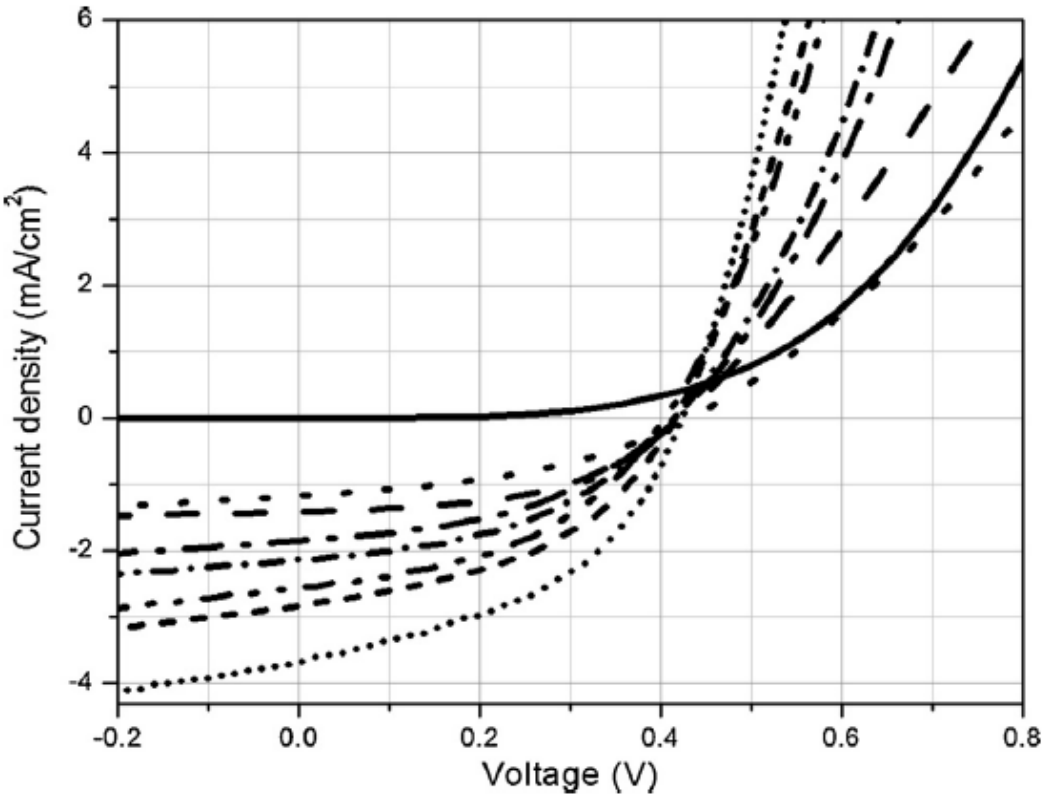

Figure 1.8 Current-Voltage plots of P3HT- ZnS dark (solid), P3HT-ZnS light (dash), P3HT-Cd-doped ZnS, 0.2 M (dot), P3HT-Cd-doped ZnS, 0.3 M (dash dot), P3HT-Cd- doped ZnS, 0.4 M (dash dot), P3HT-Cd-doped ZnS, 0.5 M (short dot), P3HT-Cd-doped ZnS, 0.6 M (short dash), P3HT-Cd-doped ZnS, 0.7 M (short dash dot) [25]

Table 1.1 Characteristics Parameters From Current Voltage Plots [25]

Solar Cell Composition	J_{sc} (mA/cm^2)	V_{oc} (V)	M_{pp} (mW/cm^2)	Fill Factor	% Efficiency
P3HT-ZnS Light	1.42	0.43	0.30	0.49	0.30 ± 0.02
P3HT-doped ZnS (0.2 M, Cd)	1.17	0.43	0.21	0.41	0.21 ± 0.02
P3HT-doped ZnS (0.3 M, Cd)	1.85	0.41	0.34	0.45	0.34 ± 0.02
P3HT-doped ZnS (0.4 M, Cd)	2.55	0.41	0.46	0.44	0.46 ± 0.02
P3HT-doped ZnS (0.5 M, Cd)	3.69	0.43	0.69	0.44	0.70 ± 0.02
P3HT-doped ZnS (0.6 M, Cd)	2.83	0.42	0.52	0.43	0.51 ± 0.02
P3HT-doped ZnS (0.7 M, Cd)	2.13	0.41	0.39	0.42	0.38 ± 0.02

D.J. Lee et al. also fabricated almost this type of hybrid cells with ZnCdS NWs as inorganic semiconductor synthesized by vacuum assisted co-evaporation technique from ZnS and CdS grains. While the solar cell device fabrication method is almost the same as above. D J Lee et al studied the effect of light intensity and temperature on the efficiency of the device. The following **Figure 1.9** shows the schematic energy level diagram of the fabricated hybrid heterostructure solar cell (under illumination) that explains the transfer photogenerated electrons and holes to take place across the interface between conjugated polymer and semiconducting NWs. This could be attributed to the higher electron affinity (E_{ea}~3.2 eV) of P3HT molecules, which help in transferring the electron into the 1D wires that possess a relatively lower electron affinity (_4.0 < E_{ea} < ~3.0 eV) and Eg around 3.4 eV. Also, in this case both P3HT and ZnCdS systems could have played an active role in generating the electron-hole pairs (under illumination) required for the carrier dynamics of the device.

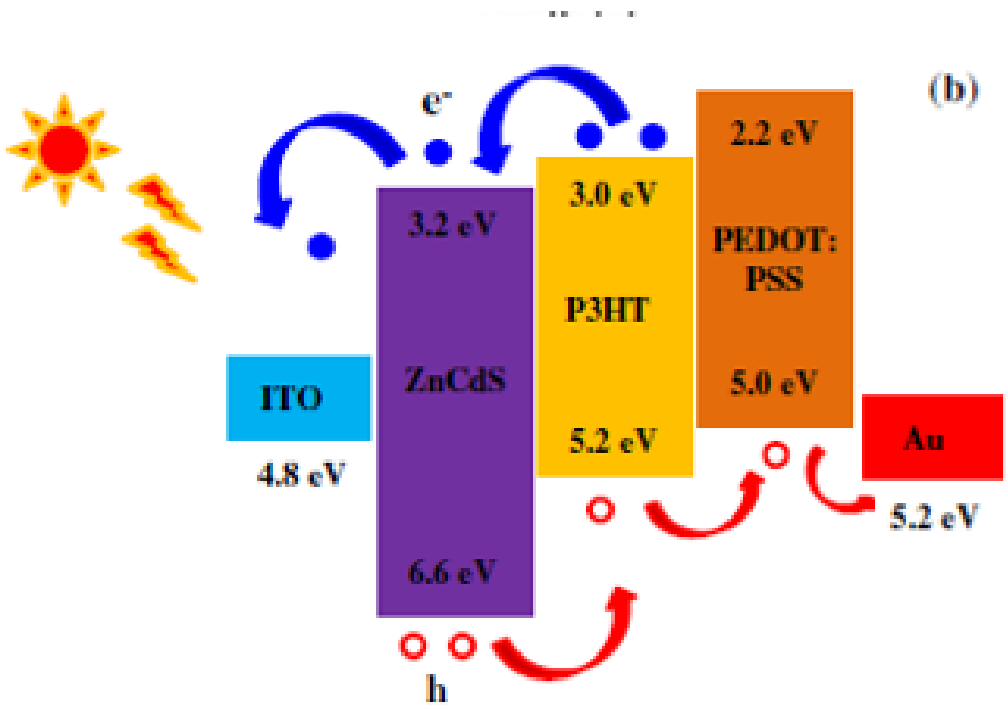

Figure 1.9 Schematic energy level diagram of the ZnCdS/P3HT based hybrid heterostructure under illumination [60]

1.10.3 Photocatalyst

ZnS is a wide band gap semiconductor having remarkable chemical stability towards oxidation and hydrolysis. The properties are retained even when the particle size is decrease to a few nanometers. This make the ZnS nanostructures an interesting materials for catalytic activities where they would to expose to aggressive environments. The electronic properties and band gap can be modified with incorporation of other elements like making $Zn_{1-x}Cd_xS$ ternary sulfides. These nanostructure have been used for photocatalytic degradation of toxic organic pollutants such as dyes, p-nitrophenol and halogenated benzene derivatives in waste water treatment and also in photocatalytic water splitting for hydrogen production due to rapid generation of electron hole pairs by photoexcitation and because of high negative reduction potentials of excited electrons.

1.10.3.1 As a Photocatalyst for Hydrogen Production From H_2S

The world is facing the issue of energy crises due to the depletion of fossil fuels reserves as well as the problem of environmental pollution due the continuous burning of fossil fuel resources containing very large amount of sulfur compound. Highly toxic and corrosive hydrogen sulfide is continuously emitted out to the environment by the oil refineries in huge amount (15-20 %) and is global threat to the environment. So the hydrogen is an alternative attractive sustainable source for the fossil fuels. Therefore the H_2 production is of great interest from H_2S because of possible application for converting sunlight energy into chemical energy [61].

S.N.Garaje et al. synthesized nanostructured $Zn_{1-x}Cd_xS$ by solid-solid phase reaction method using ZnO, CdO and thiourea as sources of Cd, Zn and S respectively. The synthesized nanostructure with tunable band gap was used as photocatalyst for H_2 evolution form H_2S gas. For the experiment 0.5 g of the catalyst in 750 mL KOH solution (0.5M) were used with H_2S flow 2.5mL min^{-1} in cylindrical quartz reactor and a Xe-lamp of 450 W was used as light source. The excess of H_2S was trapped in NaOH solution while the hydrogen gas evolved was measured using a graduated gas burette and analyzed by gas chromatograph [61].

The rates of hydrogen evolution for synthesized $Zn_{1-x}Cd_xS$ nanostructures and bulk CdS is given the following table. It is clear from the **Table 1.2** that $Zn_{0.9}Cd_{0.1}S$ nanostructure

exhibit the highest activity for hydrogen production that is 8320 μmol $h^{-1}g^{-1}$ under the visible light irradiation which is higher than that of bulk CdS. The highest activity of H_2 production may attributed to $Zn_{0.9}Cd_{0.1}S$ that possess an optimum band gap and moderate position of the conduction band with appropriate amount Zn into the lattice of CdS provides suitable impurity levels which make the excited electron from the valence band of the CdS to easily inject into the conduction band.

Table 1.2 photocatalytic Activities of H_2 Evolution from H_2S [61]

S/No	Samples	Rate of H_2 evolution (µmol h^{-1} g^{-1})
1	$Cd_{0.1}Zn_{0.9}S$	8320
2	$Cd_{0.5}Zn_{0.5}S$	7400
3	$Cd_{0.9}Zn_{0.1}S$	6300
4	Nanostructured CdS	5890
5	Bulk CdS	2020

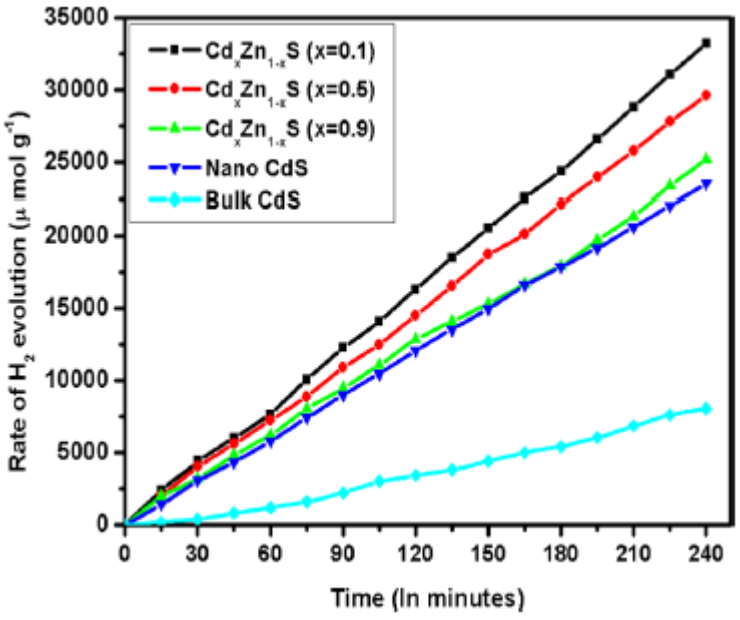

Figure 1.10 photocatalytic activities for H_2 production by as synthesized $Zn_{1-x}Cd_xS$ nanostructures and bulk CdS [61]

1.10.3.2 As a Catalyst For H_2 Production From Photocatalytic Water Splitting

Numerous active photocatalyst such as various oxides, sulfides and oxynitride semiconductors have been developed for photocatalytic water splitting for H_2 production. Among them, Metal sulfides and their composite are good candidates for the aforementioned photocatalytic reaction. Particularly, ZnS is one of the most used photocatalyst due to rapid generation of electron-hole pairs upon photoexcitation and high reduction potential of excited electrons. It shows high photocatalytic activity for H_2 production even without noble metal as cocatalayst in the UV- light irradiation. The only limitation is its too large high band gap to respond to the visible light. In order to decrease its band to visible region many attempts have been made to develop doped ZnS and also to prepare its solid solution (like $Zn_{1-x}Cd_xS$, Cu- $Zn_{1-x}Cd_xS$ and CuS-In_2S_3-ZnS etc.). These ZnS based solid solution have proven to be efficient, low toxic and cost effective visible light responsive photocatalyst for H_2 production from water splitting [62].

J. Zhang et al. synthesize nanocomposite of $Zn_{1-x}Cd_xS$ with reduced graphene oxide (RGO) by co-precipitation hydrothermal method using $Cd(Ac)_2.2H_2O$, $Zn(Ac)_2.2H_2O$ and Na_2S as the corresponding precursors in the presence of GO. The synthesized nanocomposites was used as photocatalyst for hydrogen production from water splitting using Na_2S and Na_2SO_3 as sacrificial agent which scavenge hole and also suppress the oxidation of S^{-2} on $Zn_{0.8}Cd_{0.2}S$ surface. The optimized RGO- $Zn_{0.8}Cd_{0.2}S$ showed high H_2 production rate of 1824μmol h^{-1} g^{-1} at the RGO content of 0.25 wt % and the apparent quantum efficiency of 23.4 % at 420 nm. The result display significantly enhanced H_2 production in comparison with pristine $Zn_{0.8}Cd_{0.2}S$ as well as better than that of Pt- $Zn_{0.8}Cd_{0.2}S$ under the same reaction conditions shows that RGO- $Zn_{0.8}Cd_{0.2}S$ nanocomposite represent one of the most highly efficient metal sulfide photocatalyst in the absence of noble metal cocatalyst [62].

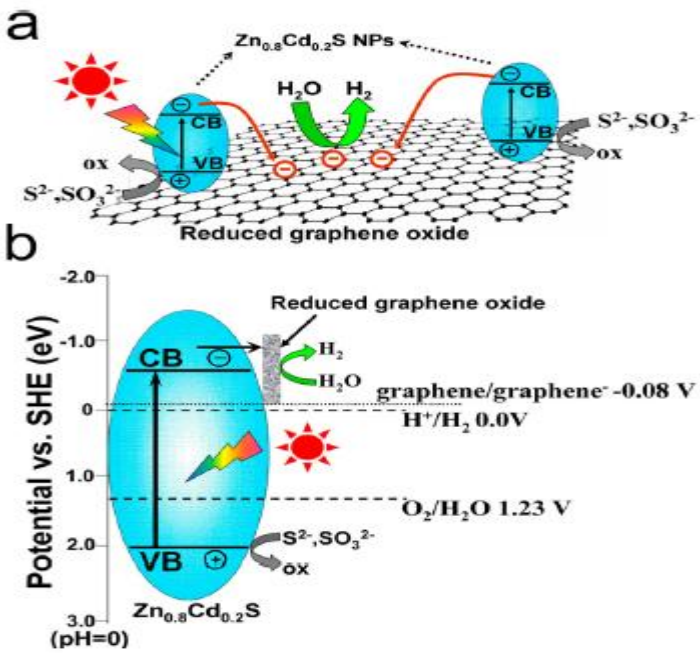

Figure 1.11 (a) schemetic representation of charge trasfer and charge separation in reduce graphene oxide- $Zn_{0.8}Cd_{0.2}S$ nanocomposite, (b) Suggested mechanism for H_2 production under solar light irridiation using reduce graphene oxide- $Zn_{0.8}Cd_{0.2}S$ nanocomposite as a photocatalyst [62]

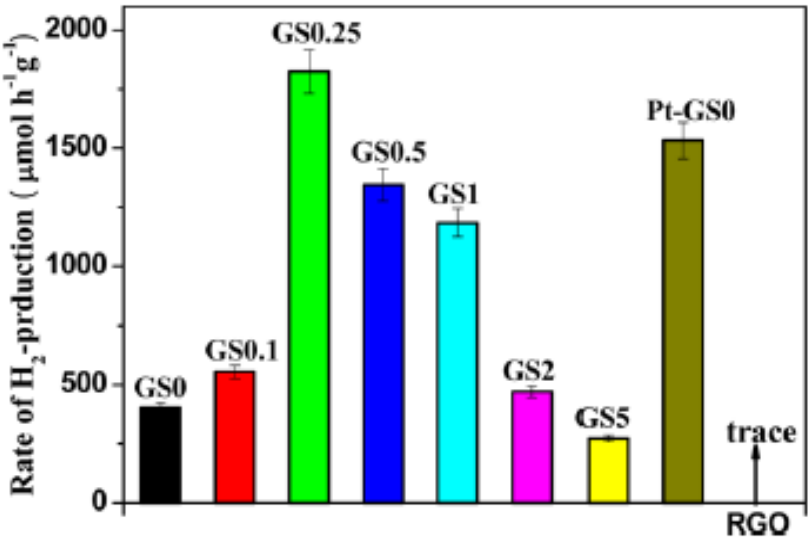

Figure 1.12 Comparison of H_2 production rates using various synthesized RGO- $Zn_{0.8}Cd_{0.2}S$ nanocomposite as photocatalyst with different RGO wt. % (0.0, 0.1, 0.25, 0.5, 1, 2, 5) , Pt-RGO [62]

The result shows that RGO- $Zn_{0.8}Cd_{0.2}S$ nanocomposite show higher activity then pristine $Zn_{0.8}Cd_{0.2}S$ and similarly increase in the photocatalytic activity is observed with increase in wt % of RGO in nanocomposite which reach to a maximum limit for 2.5% of RGO and further increase its amount decrease the photocatalytic activity which may be due to the two possible reasons.(a) The incorporation of black RGO in large amount may results in shielding the incident light which leads to the inhibition electron generation inside the $Zn_{0.8}Cd_{0.2}S$ nanostructure. (b) Similarly the excess amount of the RGO may cover the surface active sites of $Zn_{0.8}Cd_{0.2}S$ nanostructure and thus could prevent the contact of sacrificial agent with $Zn_{0.8}Cd_{0.2}S$ nanostructure [62].

D.H.Wang et al. synthesized a series of $Zn_{1-x}Cd_xS$ solid solution with nanoporous structure. The synthesized solid solution nanostructures shows efficient photocatalytic activity for hydrogen generation from water splitting. The photocatalytic activity was carried out in aqueous solutions having S^{2-} and SO_3^{2-} as sacrificial agent under the Xe-Lamp as visible light source also using Pt as a cocatalyst to improve the photocatalytic activity. The synthesized photocatalyst with x = 0.2 at neutral pH (7.3) show highest photocatalytic activity which was further enhance by loading Pt 0.25 wt% as cocatalyst from 193 μmol h^{-1} to 458 μmol h^{-1}. The photocatalytic activity of $Zn_{0.8}Cd_{0.2}S$ solid solution may be attributed to the visible light absorption because of incorporation of Cd and to the relatively negative conduction band potential due the high content of Zn in the solid solution [63].

1.10.3.3 As a Photocatalyst for Photodegradation of Organic Pollutants

1.10.3.3a Introduction to Organic Pollutants

Water contamination due to hazardous water soluble organic dyes and chemicals poses a severe risk to the environment [64].The surplus azo dyes in effluents from textile and dyeing industries are commonly resistant to biodegradation. These colored compounds disturb aquatic biological processes either by blocking light penetration or direct destruction of aquatic communities due to associated noxiousness. As they contain large degree of organics and shows higher stability, these contaminants pose severe ecological problems by depleting the dissolved oxygen content of water and discharging toxic compounds that put in danger the aquatic life. During an anaerobic treatment, these azo dyes may generate cancer-causing (carcinogenic) compounds such as aromatic amines. Due to this, purification

and detoxification of industrial waste water has been one of the most important challenges [65]. To find an effective and long lasting solution for the removal of these aquatically harmful compounds a range of technologies have been tested which include biodegradation, adsorption, filtration, sedimentation and photocatalytic degradation [66-68].Photocatalytic degradation, in which the organic pollutants are degraded through photocatalytic oxidation and reduction reactions in the presence of a photocatalyst is one of the most likely and clean methods used for water purification [69].

Organic dyes are one of the major groups of pollutants added into waste water from textile and other industrial processes [70, 71]. Effective removal of organic dyes from aquatic environments is of vital significance not only for water purification and conservation but also for preserving human and ecological health [72]. Photocatalysis is becoming a worthwhile approach for the degradation of organic dyes (such as methylene blue a cationic dyes) in waste water with the employment of solar energy [72, 73] .So far, many semiconducting materials, such as TiO_2, ZnS, CdS and $Zn_{1-x}Cd_xS$, have been intensively established as photocatalysts for environmental sanitization applications [73]. Among them, ternary $Zn_{1-x}Cd_xS$ alloy semiconductor has been extensively studied both in theory and experiment due to its tunable bandgap for effective application of visible light [74].

1.10.3.3bVarious Techniques for the Degradation and Decoloriztion of the Organic Dyes

The complete degradation of the dyes is not possible by conventional methods such as precipitation, adsorption, flocculation, flotation, oxidation, reduction, electrochemical, aerobic, anaerobic, and biological treatment methods. These methods have inherent limitations in technologies such as less efficiency and production of secondary sludge, the disposal of which is a costly affair [75-79]. Merely, transferring hazardous materials from one medium to another is not a long-term solution to the issue of toxic waste loading on the environment. Many technologies have been applied to remedy dyes from wastewater, like coagulation/flocculation, biological treatment, electrochemical, membrane filtration, ion exchange, adsorption, and chemical oxidation [80, 81].

Chemical coagulations for dye removal require loading of chemical coagulating agent and optimal operating conditions like pH and coagulation dosage should be rigidly reminded for achieving maximum dye removal [82]. The coagulation flocculation process can be utilized as a pre- or post- or even as a main treatment. This process is cost effective and easy as it consumes less energy than the conventional coagulation treatment .However, utilizing inorganic salts like aluminum chloride and aluminum sulfate as the coagulation agent has now become controversial because of their possibility of contributing to Alzheimer's disease. Polyacrylamide-based materials are also often utilized in the coagulation process, but the possible release of monomers is now considered damaging due to their entering into the food chain and causing potential health impacts (e.g., carcinogenic effects) [83]. Adsorption removal method is a simple and effective method/design since it is easy to use and can be implemented for dye treatment even in small plants; however, it usually produces huge amounts of sludge, especially in the wastewater with high dye concentrations. Adsorption of dyes on many adsorbents (e.g., SiO_2, Al_2O_3, CaO, MgO, Fe_2O_3, Na_2O, K_2O, bentonite, and montmorillonite) has been broadly studied, but the activated carbon has been proven to be the most effective catalyst due to its high specific surface area, ultra-high adsorption capacity, and low selectivity for both nonionic and ionic dyes. However, it has some limitations, including the need for regeneration after exhausting, high cost of the activated carbon, and the lack of adsorption efficiency after regeneration [84].

Taking all these facts into consideration, much of the present work involves the degradation and mineralization of synthetic dyestuff in industry by heterogeneous photocatalyst. The heterogeneous photocatalyst relates to the water decontamination processes that are concerned with the oxidation of non-biodegradable organic compounds. This impressive method relies on the formation of highly reactive chemical species that degrade a number of recalcitrant molecules into biodegradable compounds and is known as the advanced oxidation process (AOP). The Environmental Protection Agency (EPA) has approved the inclusion of AOP as the best available technology to meet the standard with specifications that provide safe and sufficient pollution control of industrial processes and remediation of contaminated sites. Advanced oxidation processes are based on the production of hydroxyl radicals which oxidize a wide range of organic pollutants including dyes quickly and nonselectively [85].

AOPs include homogenous and heterogeneous photocatalytic oxidation systems. The homogenous photocatalytic oxidation system employs various oxidants such as H_2O, O_3, Fenton reagent, NaOCl, and many others either alone or in combination with light **Figure 1.13**. Recently, heterogeneous photocatalysis has emerged as an important degradation technology leading to the total mineralization of organic pollutants, especially synthetic dyes.

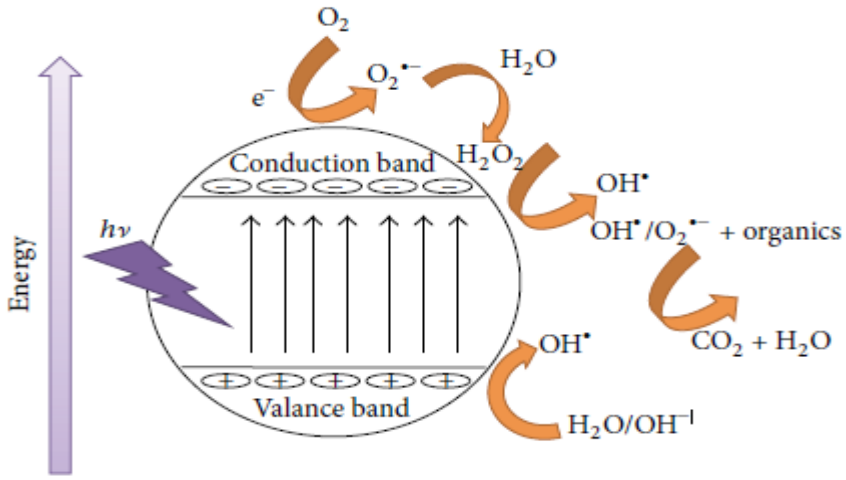

Figure 1.13 General view on photocatalytic mechanism and degradation process [85]

1.10.4 Some Other Applications

Due to the luminescence and nonlinear optical properties, quantum size effect, and other excellent physical and chemical properties, nanocrystalline semiconductors of groups II-VI have also potential applications in various other technical fields like biological detection and imaging, photodetectors and UV sensors, nonlinear optical materials, short-wavelength laser diodes, various luminescence devices, etc. [25].

References

1. Xia Y, Yang P, Sun Y, Wu Y, Mayers B, Gates B, et al. One-dimensional nanostructures: synthesis, characterization, and applications. *Adv. mater.* **2003**,15,353-89.
2. Fang X, Bando Y, Gautam UK, Ye C, Golberg D. Inorganic semiconductor nanostructures and their field-emission applications. J. Mater. Chem. **2008**,18,509-22.
3. Zhai T, Fang X, Li L, Bando Y, Golberg D. One-dimensional CdS nanostructures: synthesis, properties, and applications. *Nanoscale.* **2010**,2,168-87.
4. Fang X, Bando Y, Gautam UK, Zhai T, Zeng H, Xu X, et al. ZnO and ZnS nanostructures: ultraviolet-light emitters, lasers, and sensors. *Crit. Rev. Solid State Mater. Sci.* **2009**,34,190-223.
5. Kuchibhatla SV, Karakoti A, Bera D, Seal S. One dimensional nanostructured materials. *Prog. Mater. Sci.* **2007**,52,699-913.
6. Davidson, W. In X-ray diffraction evidence for ZnS formation in zinc activated rubber vulcanizates, *Phys. Rev.* **1948**,116-117.
7. Fang X, Zhai T, Gautam UK, Li L, Wu L, Bando Y, et al. ZnS nanostructures: from synthesis to applications. *Prog. Mater. Sci.* **2011**,56,175-287.
8. Yeh C-Y, Lu Z, Froyen S, Zunger A. Zinc-blende–wurtzite polytypism in semiconductors. *Phys. Rev. B.* **1992**,46,10086.
9. Harrison M, Kershaw S, Burt M, Eychmüller A, Weller H, Rogach A. Wet chemical synthesis and spectroscopic study of CdHgTe nanocrystals with strong near-infrared luminescence. *Mater. Sci. Eng.B.* **2000**,69,355-60.
10. Wang W, Germanenko I, El-Shall MS. Room-Temperature Synthesis and Characterization of Nanocrystalline CdS, ZnS, and $Cd_xZn_{1-x}S$. *Chem. Mater.* **2002**,14,3028-33.
11. Kulkarni S, Winkler U, Deshmukh N, Borse P, Fink R, Umbach E. Investigations on chemically capped CdS, ZnS and ZnCdS nanoparticles. *Appl. Surf. Sci.***2001**,169,438-46.

12. Petrov D, Santos B, Pereira G, de Mello Donegá C. Size and Band-Gap Dependences of the First Hyperpolarizability of Cd_x $Zn_{1-x}S$ Nanocrystals. *J. Phys. Chem. B.* **2002**,106,5325-34.
13. Bailey RE, Nie S. Alloyed semiconductor quantum dots: tuning the optical properties without changing the particle size. *J. Am. Chem. Soc*. **2003,**125,7100-6.
14. Zhong X, Han M, Dong Z, White TJ, Knoll W. Composition-Tunable $Cd_xZn_{1-x}Se$ Nanocrystals with High Luminescence and Stability. *J. Am. Chem. Soc.* **2003**,125,8589-94.
15. Weller H. Quantized semiconductor particles: a novel state of matter for materials science. *Adv. Mater.* **1993**,5,88-95.
16. Youn HC, Baral S, Fendler JH. Dihexadecyl phosphate, vesicle-stabilized and in situ generated mixed cadmium sulfide and zinc sulfide semiconductor particles: preparation and utilization for photosensitized charge separation and hydrogen generation. *J. Phys. Chem.***1988**,92,6320-7.
17. Kumar A, Jakhmola A, Chaudhary V. Synthesis and photophysics of colloidal ZnS/PbS/ZnS nanocomposites—An analysis of dynamics of charge carriers. *J. Photochem. Photobiol. A: Chem.* **2009**,208,195-202.
18. Lifshitz E, Porteanu H, Glozman A, Weller H, Pflughoefft M, Echymüller A. Optically detected magnetic resonance study of CdS/HgS/CdS quantum dot quantum wells. *J. Phys. Chem. B.* **1999**,103,6870-5.
19. Li Y, Feng J, Daniels S, Pickett NL, O'Brien P. A highly luminescent ZnS/CdSe/ZnS nanocrystals-tetrapeptide biolabeling agent. *J. nanosci. nanotechnol.* **2007**,7,2301-8.
20. Murugadoss G. Luminescence properties of multilayer coated single structure ZnS/CdS/ZnS nanocomposites. *Spectrochim. Acta, Part A.* **2012**,93,53-7.
21. Muruganandham M, Kusumoto Y. Synthesis of N, C codoped hierarchical porous microsphere ZnS as a visible light-responsive photocatalyst. *J. Phys. Chem. C.* **2009**,113,16144-50.
22. Wang G, Huang B, Li Z, Lou Z, Wang Z, Dai Y, et al. Synthesis and characterization of ZnS with controlled amount of S vacancies for photocatalytic H_2 production under visible light. *Sci. Rep*. **2015**,5.

23. Revathi R, Kutty T. Blue ac electroluminescence of $Zn_{1-x}Mg_xS$: Cu, Br powder phosphors. *J. mater. sci.* **1986**,21,2100-8.
24. Huang J, Yang Y, Xue S, Yang B, Liu S, Shen J. Photoluminescence and electroluminescence of ZnS: Cu nanocrystals in polymeric networks. *Appl. phys. lett*. **1997**,70,2335-7.
25. Jabeen U, Shah SM, Hussain N, Ali A, Khan SU. Synthesis, characterization, band gap tuning and applications of Cd-doped ZnS nanoparticles in hybrid solar cells. *J. Photochem. Photobiol. A*: *Chemi*.**2016**,325,29-38.
26. Kishimoto S, Hasegawa T, Kinto H, Matsumoto O, Iida S. Effect and comparison of co-doping of Ag, Ag+ In, and Ag+ Cl in ZnS: N/GaAs layers prepared by vapor-phase epitaxy. *J. cryst.growth*. **2000**,214,556-61.
27. Ollinger M, Craciun V, Singh R. Nanoencapsulation of ZnS: Ag particulates with indium tin oxide for field emission displays. *Appl. physi. lett*. **2002**,80,1927-9.
28. Korotchenkov O, Cantarero A, Shpak A, Kunitskii YA, Senkevich A, Borovoy M, et al. Doped ZnS: Mn nanoparticles obtained by sonochemical synthesis. *Nanotechnol*. **2005**,16,2033.
29. Tsujii N, Kitazawa H, Kido G. Magnetic properties of Mn-and Eu-doped ZnS nanocrystals. *J. appl. phys.* **2003**,93,6957-9.
30. Borse PH, Vogel W, Kulkarni S. Effect of pH on photoluminescence enhancement in Pb-doped ZnS nanoparticles. *J. Colloid Interface Sci.* **2006**,293,437-42.
31. Jian W, Zhuang J, Zhang D, Dai J, Yang W, Bai Y. Synthesis of highly luminescent and photostable ZnS: Ag nanocrystals under microwave irradiation. *Mater. chem. phys.* **2006,**99,494-7.
32. Wang L, Wang P, Huang B, Ma X, Wang G, Dai Y, et al. Synthesis of Mn-doped ZnS microspheres with enhanced visible light photocatalytic activity. *Appl. Surf. Sci.* **2017**,391,557-64.
33. Bruchez M, Moronne M, Gin P, Weiss S, Alivisatos AP. Semiconductor nanocrystals as fluorescent biological labels. *sci.* **1998**,281,2013-6.
34. Chan WC, Nie S. Quantum dot bioconjugates for ultrasensitive nonisotopic detection. *Sci.* **1998**,281,2016-8.

35. Plass R, Pelet S, Krueger J, Grätzel M, Bach U. Quantum dot sensitization of organic−inorganic hybrid solar cells. *J. Phys. Chem. B.* **2002**,106,7578-80.

36. Zhong X, Feng Y, Knoll W, Han M. Alloyed ZnxCd1-xS Nanocrystals with Highly Narrow Luminescence Spectral Width. *J. Am. Chem. Soc.* **2003**,125,13559-63.

37. Huang J, Lianos P, Yang Y, Shen J, Preparation of ZnxCd1-xS Nanocomposites in Polymer Matrices and Their Photophysical Properties. *Langmuir* **1998,** *14*,4342-4344.

38. Li Y, Ye M, Yang C, Li X, Li Y. Composition-and Shape-Controlled Synthesis and Optical Properties of $Cd_xZn_{1-x}S$ Alloyed Nanocrystals. *Adv. Funct. Mater.* **2005**,15,433-41.

39. Wada Y, Niinobe D, Kaneko M, Tsukahara Y. Synthesis of $Cd_xZn_{1-x}S$ Nanoparticles in Porous Vycol Glass by Reaction of Single-source Precursors. *Chem. lett.* **2005**,35,62-3.

40. Liu Y, Zapien JA, Shan Y, Geng CY, Lee CS, Lee ST. Wavelength-Controlled Lasing in $Cd_xZn_{1-x}S$ Single-Crystal Nanoribbons. *Adv. Mater.* **2005**,17,1372-7.

41. Zhai T, Gu Z, Yang W, Zhang X, Huang J, Zhao Y, et al. Fabrication, structural characterization and photoluminescence of single-crystal $Cd_xZn_{1-x}S$ zigzag nanowires. *Nanotecnol.* **2006**,17,4644.

42. Li W, Li D, Chen Z, Huang H, Sun M, He Y, et al. High-efficient Degradation of Dyes by $Zn_xCd_{1-x}S$ Solid Solutions under Visible Light Irradiation. *J. Phys. Chem. C.* **2008**,112,14943-7.

43. Li Z, Wang Y, Liu J, Chen G, Li Y, Zhou C. Photocatalytic hydrogen production from aqueous methanol solutions under visible light over Na (Bi_xTa_{1-x}) O 3 solid-solution. *Int. J. Hydrogen Energy*. **2009**,34,147-52.

44. Wang Wenzhong. Monodisperse, mesoporous $Cd_xZn_{1-x}S$ nanoparticles as stable visible-light-driven photocatalysts. **2008**.

45. Kumar V, Singh V, Sharma SK, Sharma T. Structural and optical properties of sintered $Cd_xZn_{1-x}S$ films. *Opt. Mater.* **1998**,11,29-34.

46. Lin, J.; Guo, M.; Yip, C. T.; Lu, W.; Zhang, G.; Liu, X.; Zhou, L.; Chen, X.; Huang, H., High temperature crystallization of free-standing anatase TiO_2 nanotube membranes for high efficiency dye-sensitized solar cells. *Adv. Funct.l Mater.* **2013,** *23* , 5952-5960.

47. Li Q, Meng H, Zhou P, Zheng Y, Wang J, Yu J, et al. $Cd_xZn_{1-x}S$ Solid Solutions with Controlled Bandgap and Enhanced Visible-Light Photocatalytic H_2-Production Activity. *Am. Chem.Soc. Catal.* **2013**,3,882-9.

48. Yu J, Zhang J, Jaroniec M. Preparation and enhanced visible-light photocatalytic H 2-production activity of CdS quantum dots-sensitized $Cd_xZn_{1-x}S$ solid solution. *Green Chem.* **2010**,12,1611-4.

49. Bao N, Shen L, Takata T, Domen K. Self-templated synthesis of nanoporous CdS nanostructures for highly efficient photocatalytic hydrogen production under visible light. *Chem. Mater.* **2007**,20,110-7.

50. Xu X, Lu R, Zhao X, Xu S, Lei X, Zhang F, et al. Fabrication and photocatalytic performance of a $Cd_xZn_{1-x}S$ solid solution prepared by sulfuration of a single layered double hydroxide precursor. *Appl. Catal., B: Environ.* **2011**,102,147-56.

51. Meissner D, Memming R, Kastening B, Bahnemann D. Fundamental problems of water splitting at cadmium sulfide. *Chem. phys. lett.* **1986**,127,419-23.

52. Guo L, Zhao L, Jing D, Lu Y, Yang H, Bai B, et al. Reprint of: Solar hydrogen production and its development in China. *Energy*. **2010**,35,4421-38.

53. Wang L, Wang W, Shang M, Yin W, Sun S, Zhang L. Enhanced photocatalytic hydrogen evolution under visible light over $Cd_xZn_{1-x}S$ solid solution with cubic zinc blend phase. *Int. J. Hydrogen Energy*. **2010**,35,19-25.

54. Wu J-C, Zheng J, Zacherl CL, Wu P, Liu Z-K, Xu R. Hybrid Functionals Study of Band Bowing, Band Edges and Electronic Structures of $Cd_xZn_{1-x}S$ Solid Solution. *J. Phys. Chem., C.* **2011**,115,19741-8.

55. Sung Y-M, Lee Y-J, Park K-S. Kinetic Analysis for Formation of $Cd_xZn_{1-x}Se$ Solid-Solution Nanocrystals. *J. Am.Chem. Soc.* **2006**,128,9002-3.

56. Wang X, Liu G, Wang L, Pan J, Lu GQM, Cheng H-M. TiO_2 films with oriented anatase {001} facets and their photoelectrochemical behavior as CdS nanoparticle sensitized photoanodes. *J. Mater. Chem.* **2011**,21,869-73.

57. Gaur R, Jeevanandam P. Synthesis and Characterization of $Cd_xZn_{1-x}S$ (x=0-1) Nanoparticles by Thermal Decomposition of Bis (thiourea) cadmium–zinc acetate Complexes. *Chem. Select.* **2016**,1,2687-97.

58. Zhu L, Wang Y, Zhang D, Li C, Sun D, Wen S, et al. Gas Sensors Based on Metal Sulfide $Cd_xZn_{1-x}S$ Nanowires with Excellent Performance. *Am. Chem. Soc. appl. mater. interf*ace. **2015**,7,20793-800.

59. Günes S, Sariciftci NS. Hybrid solar cells. *Inorg. Chimi. Acta.* **2008**,361,581-8.

60. Lee DJ, Kumar GM, Ilanchezhiyan P, Lee J-C, Ryu SR, Kang TW. Vertically aligned ZnCdS nanowire arrays/P3HT heterojunctions for solar cell applications. *J. Colloid. Interface Sci.* **2017**,487,73-9.

61. Garaje SN, Apte SK, Naik SD, Ambekar JD, Sonawane RS, Kulkarni MV, et al. Template-Free Synthesis of Nanostructured $Cd_xZn_{1-x}S$ with Tunable Band Structure for H_2 Production and Organic Dye Degradation Using Solar Light. *Environ. sci. technol.* **2013**,47,6664-72.

62. Zhang J, Yu J, Jaroniec M, Gong JR. Noble metal-free reduced graphene oxide-$Cd_xZn_{1-x}S$ nanocomposite with enhanced solar photocatalytic H_2-production performance. *Nano. lett.* **2012**,12,4584-9.

63. Wang D-H, Wang L, Xu A-W. Room-temperature synthesis of $Zn_{0.80}Cd_{0.20}S$ solid solution with a high visible-light photocatalytic activity for hydrogen evolution. *Nanoscale*. **2012**,4,2046-53.

64. Ajmal A, Majeed I, Malik RN, Idriss H, Nadeem MA. Principles and mechanisms of photocatalytic dye degradation on TiO_2 based photocatalysts: a comparative overview. *Rsc Adv.* **2014**,4,37003-26.

65. Zhu H, Jiang R, Xiao L, Chang Y, Guan Y, Li X, et al. Photocatalytic decolorization and degradation of Congo Red on innovative crosslinked chitosan/nano-CdS composite catalyst under visible light irradiation. *J. Hazard. Mater.* **2009**,169,933-40.

66. El-Naas MH, Al-Muhtaseb SA, Makhlouf S. Biodegradation of phenol by Pseudomonas putida immobilized in polyvinyl alcohol (PVA) gel. *J. Hazard. Mater.* **2009,**164,720-5.

67. Hu J, Song Z, Chen L, Yang H, Li J, Richards R. Adsorption properties of MgO (111) nanoplates for the dye pollutants from wastewater. *J. Chem. Eng. Data*. **2010**,55,3742-8.

68. Cho S, Jang J-W, Kim J, Lee JS, Choi W, Lee K-H. Three-dimensional type II ZnO/ZnSe heterostructures and their visible light photocatalytic activities. *Langmuir*. **2011**,27,10243-50.

69. Kuriakose S, Bhardwaj N, Singh J, Satpati B, Mohapatra S. Structural, optical and photocatalytic properties of flower-like ZnO nanostructures prepared by a facile wet chemical method. *Beils. J. Nanotechnol*. **2013**,4,763-70.

70. Lam S-M, Sin J-C, Abdullah AZ, Mohamed AR. Degradation of wastewaters containing organic dyes photocatalysed by zinc oxide, *Desalination. Water Treatment.* **2012**,41,131-69.

71. Han F, Kambala VSR, Srinivasan M, Rajarathnam D, Naidu R. Tailored titanium dioxide photocatalysts for the degradation of organic dyes in wastewater treatment, *Appl. Catal., A: Gen.* **2009**,359,25-40.

72. Joseph JM, Destaillats H, Hung H-M, Hoffmann MR. The sonochemical degradation of azobenzene and related azo dyes: rate enhancements via Fenton's reactions. *J. Phys. Chem., A.* **2000**,104,301-7.

73. Chong MN, Jin B, Chow CW, Saint C. Recent developments in photocatalytic water treatment technology: a review. *Water Res.* **2010**,44,2997-3027.

74. Lou S, Wang W, Jia X, Wang Y, Zhou S. A unique nanoporous graphene-ZnxCd1−xS hybrid nanocomposite for enhanced photocatalytic degradation of water pollutants. *Ceram. Int.* **2016**,42,16775-81.

75. Jie R, Guo G, Zhao W, An S. Preparation and photocatalytic degradation of methyl orange of nano-powder TiO_2 by hydrothermal method supported on activated carbon. *J. Synth. Cryst.* **2013**,42,2144-9.

76. Pant B, Pant HR, Barakat NA, Park M, Han T-H, Lim BH, et al. Incorporation of cadmium sulfide nanoparticles on the cadmium titanate nanofibers for enhanced organic dye degradation and hydrogen release. *Ceram. Int*. **2014**,40,1553-9.

77. Prasannan A, Imae T. One-pot synthesis of fluorescent carbon dots from orange waste peels. *Ind. Eng. Chem. Res.* **2013**,52,15673-8.

78. Nenavathu BP, Rao AK, Goyal A, Kapoor A, Dutta RK. Synthesis, characterization and enhanced photocatalytic degradation efficiency of Se doped ZnO nanoparticles using trypan blue as a model dye. *Appl. Catal., A, General*. **2013**,459,106-13.

79. Hu SJ, Yang J, Liao XH, editors. Highly Efficient Degradation of Methylene Blue on Microwave Synthesized $FeVO_4$ Nanoparticles Photocatalysts under Visible-Light Irradiation. *Appl. Mech. Mater.* **2013**, Trans Tech Publ.
80. Aazam E, Mohamed R. Environmental remediation of Direct Blue dye solutions by photocatalytic oxidation with cuprous oxide. *J. Alloys. Compd.*. **2013**,577,550-5.
81. Xu M, Guo J, Cen Y, Zhong X, Cao W, Sun G. Shewanella decolorationis sp. nov., a dye-decolorizing bacterium isolated from activated sludge of a waste-water treatment plant. *Int. J. Syst. Evolutionary Microbiol*. **2005**,55,363-8.
82. Sakkayawong N, Thiravetyan P, Nakbanpote W. Adsorption mechanism of synthetic reactive dye wastewater by chitosan. *J. Colloid. Interface. Sci.* **2005**,286,36-42.
83. Wang Y, Wang G, Wang H, Liang C, Cai W, Zhang L. Chemical-template synthesis of micro/nanoscale magnesium silicate hollow spheres for waste-water treatment. *Chem.,A Eur. J.* **2010**,16,3497-503.
84. Gong J-L, Wang B, Zeng G-M, Yang C-P, Niu C-G, Niu Q-Y, et al. Removal of cationic dyes from aqueous solution using magnetic multi-wall carbon nanotube nanocomposite as adsorbent. *J. Hazard. Mater.* **2009**,164,1517-22.
85. Zhang S, Li J, Zeng M, Zhao G, Xu J, Hu W, et al. In situ synthesis of water-soluble magnetic graphitic carbon nitride photocatalyst and its synergistic catalytic performance. *ACS appl. mater. interface.* **2013**,5,12735-43.

Chapter 02 Experimental and Characterization

2.1 Chemicals

All chemicals used in the experiments were of analytical grade and were used without further purification. $Cd(NO_3)_2.4H_2O$, $Zn(NO_3)_2.6H_2O$, $Pb(NO_3)_2$, were purchased from Merck, NaOH from Fluka while ($(CH_3)_2NH$) 26 % and methylenblue dye (MB) was obtained from Sigma Aldrich.

All solvents were of analytical grade. Methanol and acetone were purchased from Dae Jung while CS_2 and Octylamine from Sigma Aldrich.

2.2 Synthesis of Ligand (Sodiumdimethyldithiocarbamate)

Dithiocarbamtes ligand was synthesized by a reported method [1]. Synthesis of the ligands were carried out by reaction of dimethylamine with NaOH followed by subsequent addition of CS_2 in the presence of methanol as a solvent at 0 ^oC. The presence of sulfur as a donor atom makes the dithiocarbamate a viable ligand. For the typical synthesis 37 mmol (7.2 ml, 26 % pure) of dimethylamine were dissolved in 25 mL methanol and equivalent moles of NaOH was added to this reaction mixture followed by dropwise addition of stoichiometric amount of CS_2 at temperature 0^oC along with constant stirring for four hours. The final solution was rotary evaporated and was dried substantially at room temperature to get sodium salt of dimethyldithiocarbamate **(Scheme 1).**

2.3 Synthesis of Single Source Precursor (Complexes)

Single source precursor zinc cadmium bis(N,N-dimethydithiocarbamate), $Zn_{1-x}Cd_x$-$(DMDTC)_2$ with yield of above 70 % were synthesized as follows. Appropriate molar ratio of $Zn(NO_3)_2.6H_2O$ and $Cd(NO_3)_2.4H_2O$ with sum of Zn^{2+} and Cd^{2+} 1.72 mmol and 3.45 mmol of $(CH_3)_2NCS_2Na$ were first dissolved in 25 mL methanol, respectively. The two solutions were mixed with stirring in 250 mL flask. After it was stirred constantly for 4 hours at room temperature and pressure. The resulting white precipitate were filtered, washed with methanol and dried. The zinc complex was also prepared with same procedure but without addition of $Cd(NO_3)_2.4H_2O$ **(Scheme 1).**

2.4. Synthesis of Nanostructures

The ZnS and $Cd_xZn_{1-x}S$ nanoparticle was synthesized by thermal decomposition method. Decomposition of the self-prepared precursor was carried out in two necked flask with addition of octylamine as decomposing solvent. Reaction set up was maintained at constant stirring, smoothly and constantly rising the temperature up to decomposition temperature. The temperature of reaction media was allowed to rise up to 120° C, white and yellowish color of ZnS and $Cd_xZn_{1-x}S$ nanoparticles were obtained respectively which were dispersed in methanol and then filtered. The product was washed with methanol and dried in oven at 70 ^{0}C. H_2S was released during decomposition which was allowed to pass by side tube through $Pb(NO_3)_2$ aqueous solution and form PbS, as indication of the completion of reaction **(Scheme 1).**

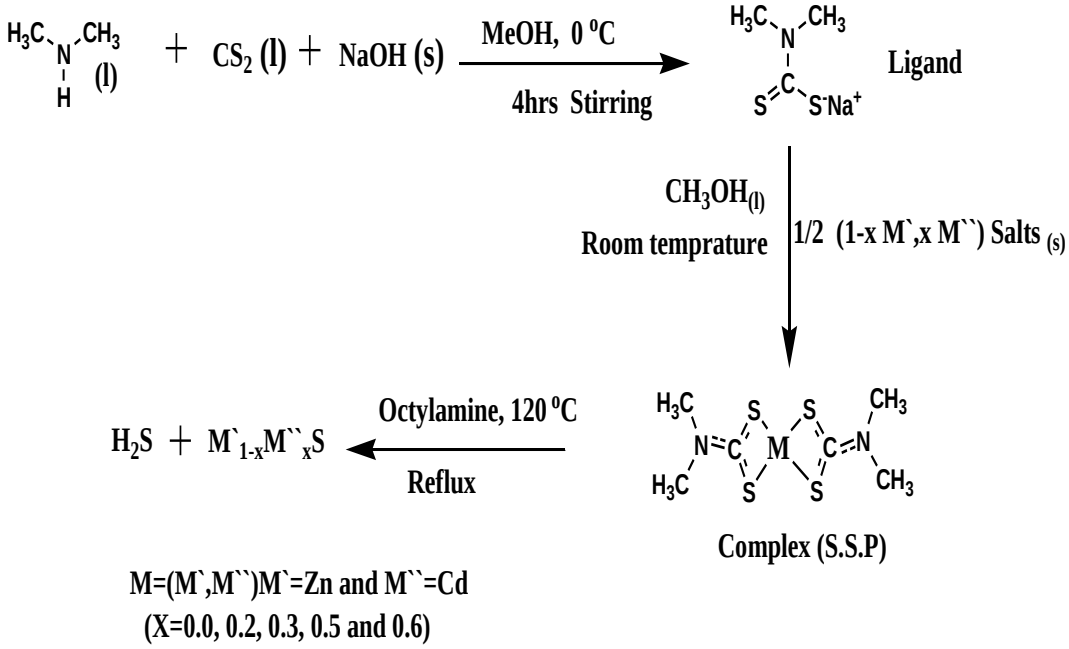

Scheme 1 Synthesis of Ligand, Complex and Nanostructures

2.5 Photocatalytic Test

The photocatalytic activities of the synthesized ZnS and $Zn_xCd_{1-x}S$ ternary sulfide nanostructures were investigated for photodegradation of methylene blue (MB) .The dye solution were prepared using distilled water. All experiments were performed in the pyrex glass vessel of 30 mL capacity containing 25 mL of 20 ppm of methylene blue solution and 15 mg of synthesized nanostructures as a photocatalyst. Prior to irradiation in each experiment the suspension was stirred in the dark for 30 minutes to establish adsorption / desorption equilibrium between the dye and catalyst surface and the change in concentration of the methylene blue due to adsorption on the catalyst surface was measured by Shimadzu 1800 spectrophotometer scanning from 200-800 nm. Magnetic stirring of the suspension was continued after exposure in sunlight to ensure the contact between the catalyst active sites and dye molecules.

The improvement of degradation and decolourization was continuously monitored with a certain time interval by withdrawing 4 mL of suspension, and analyzing the decrease in absorption, by Shimadzu 1800 spectrophotometer scanning from 200-800 nm. The (efficiency) percent degradation rate of the dye was calculated by the following equation.

$$\text{Degradation rate (\%)} = 1 - \frac{C_t}{C_o} \times 100 \qquad \textbf{(1.1)}$$

Where C_o and C_t is the initial concentration of MB dye prior to irradiation and the sample after irradiation at time T, respectively.

The kinetics of the dye degradation was expressed by Langmuir-Hinshelwood model. The reaction rate can be expressed as

$$\ln\left(\frac{C_t}{C_o}\right) = -K_{app}\, t \qquad \textbf{(1.2)}$$

Where t is the reaction time $Kapp$ is the pseudo first order kinetic constant. Plot of $\ln\left(\frac{C_t}{C_o}\right)$ vs t give $-Kapp$ [2].

2.6 Characterization

Sanyo electro thermal melting point apparatus model MP-D Mitamura Riken Kogyo (Japan) was used for determination melting point of synthesized complex and ligand using an open capillary tube. The NMR spectra were recorded on Bruker AC 300 MHz-FT-NMR spectrometer for ^{13}C and ^{1}H in solvents like MeOD and DMSO respectivily to elucidate structure of ligand and complex. Chemical shifts δ are given in ppm using TMS as internal reference. For UV-Vis DRS of synthesized nanostructure Perkin Elmer Lambda 35 Spectrometer was used. In order to find phase structure and crystallite size of ZnS and $Zn_{1-x}Cd_xS$ nanostructures, powder X-ray diffraction analysis was carried out. The analysis was performed at instrument PAN analytical X´Pert. The instrument has Cu Kά radiation wavelength 1.5418Å and values of 2 θ that was maintained from 20 to 80. Shimadzu double beam Spectrophotometer 1800 was used to monitor changes in the absorption peaks of MB dye solution during photocatalytic activity. The scanning electron microscopy images of the nanostructures and their elemental analysis were obtained on SEM JEOL Model JSM6510 coupled with Energy dispersive X-ray Spectrometer. The morphology and size of the nanostructures were investigated on a Philips EM208 transmission electron microscopy.

References

[1] Zia-ur-Rehman; Ibrahim, S.; Khan, A.; Imran, M.; Naseer, M. M.; Khan, I.; Shah, A.; Tahir, M. N.; Muneeb-ur-Rahman; Awan, I. Z., Homobimetallic zinc (II) dithiocarbamates: synthesis, characterization and in vivo antihyperglycemic activity, *J. Coord. Chem.*, **2016,** *69*, 551-561.

[2] Khan, A.; Khan, R.; Waseem, A.; Iqbal, A.; Shah, Z. H., CdS nanocapsules and nanospheres as efficient solar light-driven photocatalysts for degradation of Congo red dye. *Inorg. Chem. Commun.*, **2016,** *72*, 33-41.

Chapter 03 Results and Discussion

3.1 Physical Data of the Ligand and the Complex

Physical data of the synthesized ligand and complex are given in the **Table 3.1**. The ligand was soluble in methanol, dichloromethane and dimethyl sulfoxide with off white color while its complex with zinc was white in color and showed solubility in dimethyl sulfoxide only.

Table 3.1 Physical data of ligand and complex

Sample	Molecular formula	Physical state	Melting point ^{o}C	Solubility
Ligand	$C_3H_6NS_2Na$	Off white	120	DCM, MeOH, DMSO
Complex	$ZnC_6H_{12}N_2S_4$	White	120-130	DMSO

3.2 Structural Elucidation

For structural elucidation Nuclear Magnetic Resonance Spectroscopy was performed.

3.2.1 ^{1}H NMR Data

The ^{1}H NMR spectra of as synthesized ligand and complex were recorded on 300 MHz NMR spectrometer using methanol and DMSO as solvent respectively with TMS as a reference standard. The resonance peak in ^{1}H NMR appearing at the corresponding chemical shift and their integration value are in good agreement with composition of the compounds. The ^{1}H NMR spectra of ligand and its complex with Zn is shown in the **Figure 3.1 and 3.2** respectively.

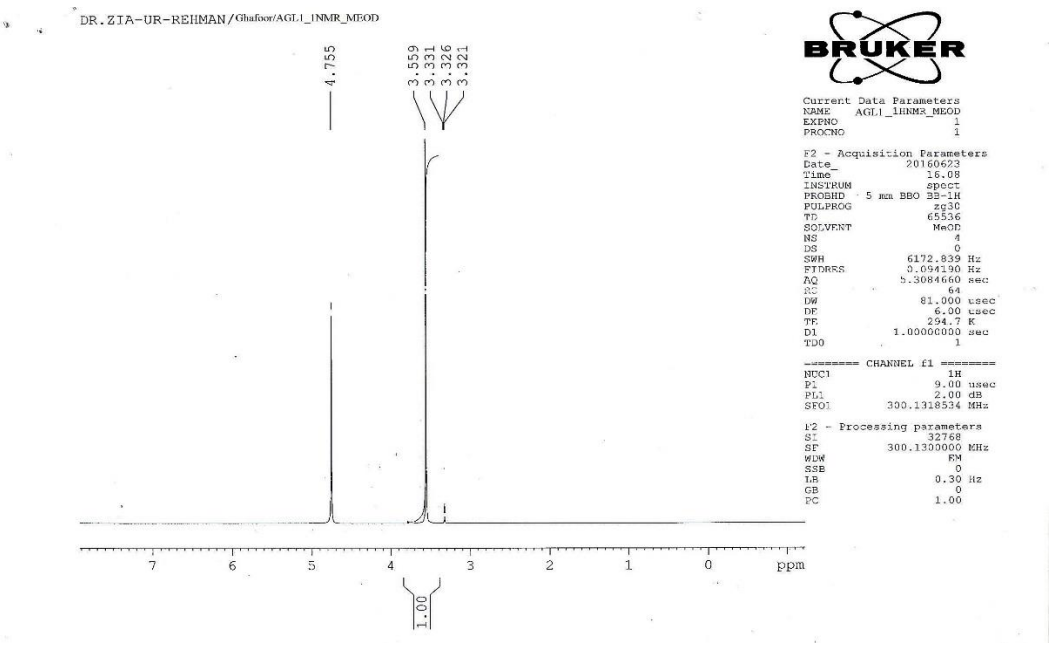

Figure 3.1 ^{1}H NMR Spectrum of the ligand

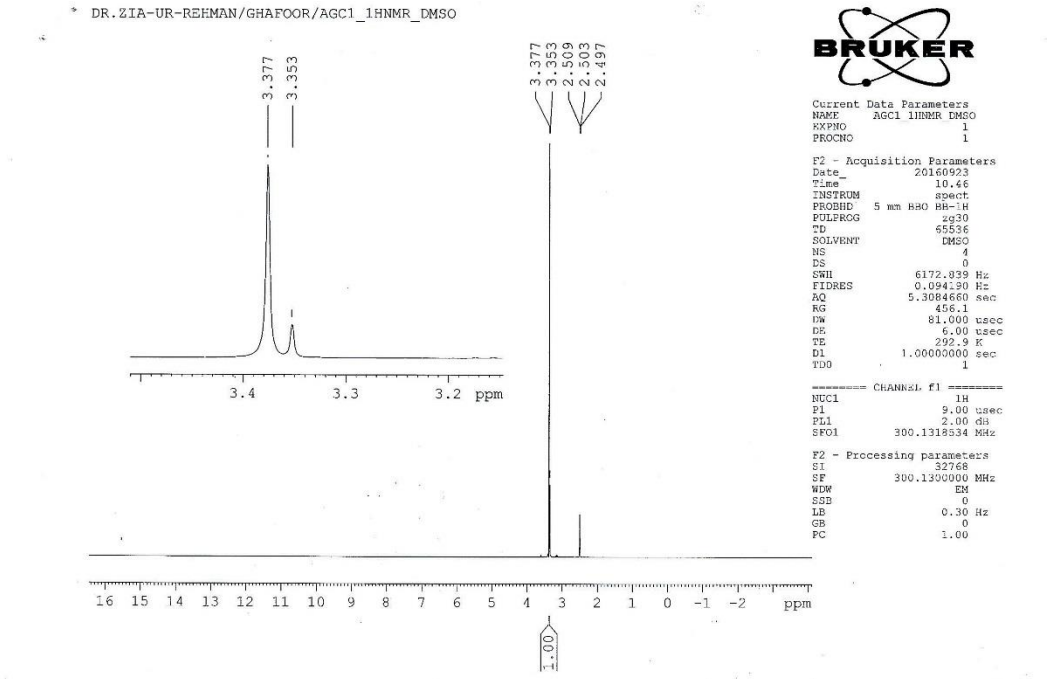

Figure 3.2 ^{1}H NMR Spectrum of the complex

3.2.2 ^{13}C NMR Data

The ^{13}C NMR spectra of the ligand and complex were recorded on 75 MHz NMR Spectrometer. The characteristic resonance peaks in the ^{13}C NMR spectra for sodiumdimethyldithiocarbamate ligand and its complex with zinc were recorded in methanol and DMSO respectively, are shown in the **Figure 3.3 and 3.4**. The chemical shift values of spectra reveals good agreement with the composition of the synthesized ligands and complex. The up field shift of CS_2 carbon δ value from 211.14 to 204.14 (ppm) and small down field shift CH_3 from 43.91 to 45.01 (ppm) was observed which indicates the coordination of the metal with ligand. This up field shift of CS_2 carbon is attributed to the shielding of CS_2 carbon and corresponding small down field shift of CH_3 carbon is due to deshielding of CH_3 carbon because of shifting of electron density (lone pair) from nitrogen towards CS_2 carbon via resonance due to coordination of ligand with the metal .[1]

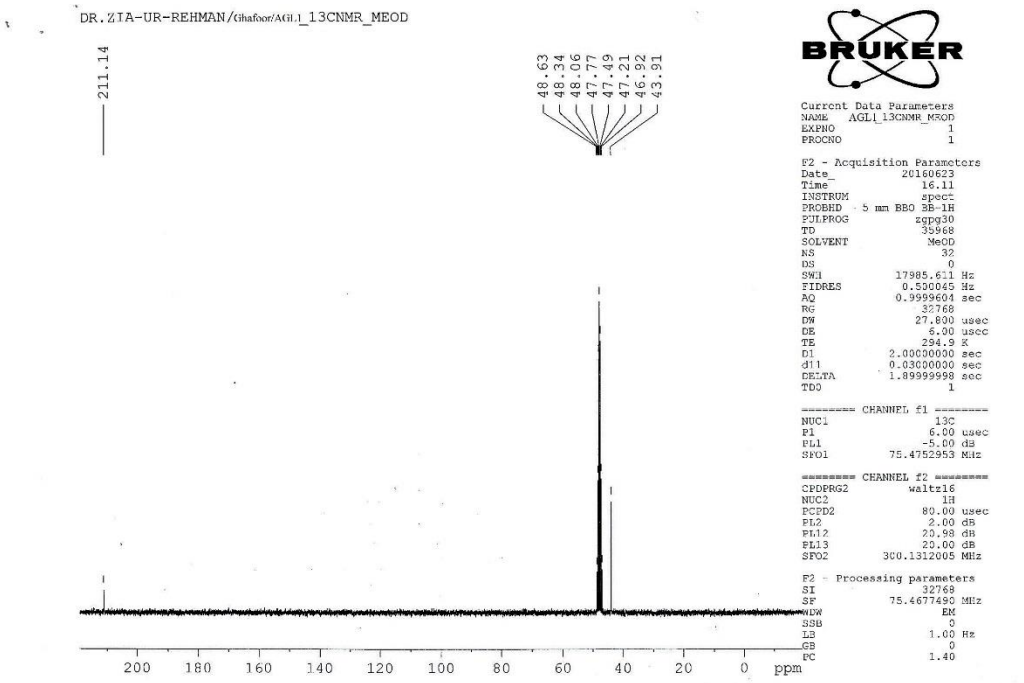

Figure 3.3 ^{13}C NMR spectrum of Ligand

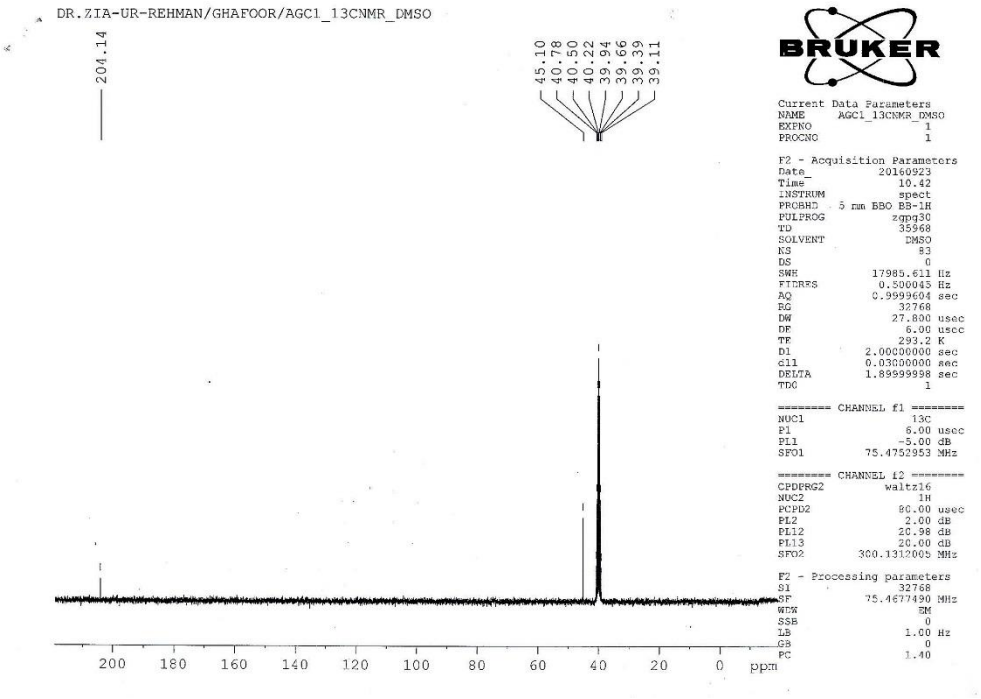

Figure 3.4 ^{13}C NMR spectrum of the Complex

3.3 UV-Visible Diffuse Reflectance Spectroscopy and Band Gap Evaluation

Comparative UV-Visible diffuse absorption spectra of synthesized nanostructured ZnS and $Zn_{1-x}Cd_xS$ (x =0.2, 0.3, 0.5, 0.6) are shown in the **Figure 3.5 (a).** An obvious and continuous red shift in the absorption onset is being observed with increasing Cd content in $Zn_{1-x}Cd_xS$ ternary sulfides nanostructure relative to the ZnS, implies incorporation of Cd in ZnS and formation of single-phase $Zn_{1-x}Cd_xS$ ternary sulfides. Similarly it also reveals that in nanostructured $Zn_{1-x}Cd_xS$ ternary sulfides the band gap can be controlled by varying Zn/Cd molar ratio using thermolysis method. The direct band gap of $Zn_{1-x}Cd_xS$ solid solution can be determined both theoretically and experimentally. By experimental method, the band gaps of the $Zn_{1-x}Cd_xS$ synthesized nanostructure were calculated using tauc plot method according to **Equation 3.1**.

$$\alpha h\upsilon = A\,(h\upsilon - E_g)^{1/2} \qquad \textbf{Eq. (3.1)}$$

Where α is the absorption coefficient, hν is the photon energy, E_g is the direct band gap, and A is a constant [2]. The **Figure 3.5 (c)** depicts that band gap energy of the synthesized

nanostructures decreases with increase in Cd content. This indicate that incorporated Cd atom in ZnS nanocrystal narrowed its band gap and extended the absorption range of ZnS into the visible region.

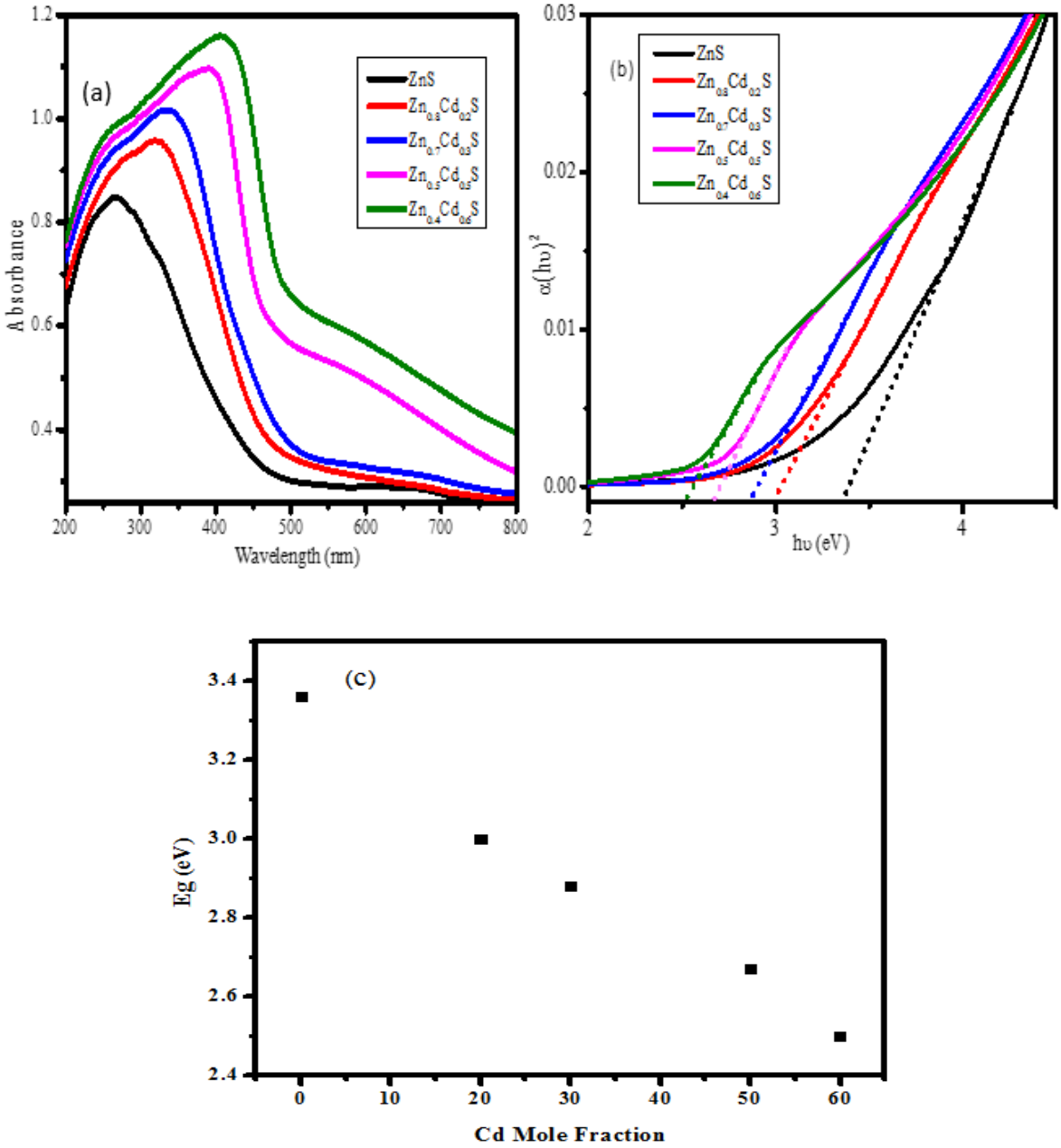

Figure 3.5 (a) UV-visible diffuse absorption spectra, (b) Tauc plots of as synthesized $Zn_{1-x}Cd_xS$ and (c) Band gap energy as a function of Cd mole fraction in $Zn_{1-x}Cd_xS$

3.4 X-ray Diffraction Analysis

Phase structure as synthesized nanostructures were characterized by the powder X- ray Diffraction (PXRD). The XRD pattern of ZnS in **Figure 6(a)** shows diffraction peaks at 2θ values 27˚,28˚,30˚,48˚,52˚and 57˚ and crystal parameters well indexed for (100), (002), (101), (110), (103) and (112) crystalline planes of hexagonal (wurtzite) ZnS with (JCPDS file # 01-0800-0007) and crystal parameters a = 3.77 and c = 6.188 Å. Similarly; for $Zn_{1-x}Cd_xS$ ternary sulfides nanostructure with highest cadmium content the relevant diffraction peaks and respective crystalline planes and crystal lattices are in good agreement with hexagonal cadmium zinc ternary sulfide with (JCPDS file # 00-040-0838) and crystal parameters a = 4.04 and c= 6.58 Å as shown in **Figure 3.6 (a).** An obvious shift in the relevant diffraction peaks of the $Cd_xZn_{1-x}S$ toward lower angle is being observed relative to the ZnS [3].

The value of electronegativity for Cd (1.69) and Zn (1.65) is approximately equal, and the radius of the Zn^{2+} ion (0.74 Å) is close to that of Cd^{2+} (0.97 Å), which facilitates the formation of solid solutions [4,5,6]. Due to relative larger size; when Cd^{2+} incorporates in to the ZnS lattice, the lattice constant would increase, which will cause the diffraction peaks to shift to lower angle. The increase in lattice constant has been observed with increasing Cd content in ternary sulfide as calculated from XRD patterns using **Equation 3.2** and plotted versus Cd mole fraction as shown in **Figure 3.6 (b).** The occurrence of the continuous peak shift clearly indicates that the obtained nanocrystals should not be the mixture of ZnS and CdS but would be $Cd_xZn_{1-x}S$ solid solution [3, 7].

$$\frac{1}{d^2} = \frac{4}{3}\left(\frac{h^2+kh+k^2}{a^2}\right) + \frac{l^2}{c^2} \qquad \textbf{(3.2)}$$

Because of comparatively small lattice mismatch between CdS and ZnS ($8^{\%}$) [8] , and the same crystal structure for ZnS and CdS proved by the XRD data, the solid solutions can easily form through the replacement of Zn with Cd.

The significant broadening of the diffraction peaks is attributed to the very small crystallite size of the obtained nanostructures. In addition to identification of the crystalline phases,

the XRD data were also used to estimate the average size of the constituent crystallites using Scherrer's equation [9].

The average grain sizes, D, were determined using **Equation (3.3):**

$$D = \frac{K\lambda}{\beta \cos\theta} \qquad \textbf{(3.3)}$$

Where λ is the wavelength of X-ray radiation (0.1541 nm), K is the Scherrer's constant (K = 0.9), θ is the diffraction angle and β is the full-width-at-half-maximum of the (002) plane (in radian).The mean crystallite sizes calculated for the $Zn_{1-x}Cd_xS$ nanostructure and lattice parameters are shown in **Table 3.2**.

Table 3.2 Lattice Parameter and Crystallite Size of Synthesized Nanostructures with Lattice Parameters of Hexagonal ZnS and $Zn_{1-x}Cd_xS$ with JCPDS file # (01-0800-0007) and (00-040-0838 respectively).

Sample	a(Å)	c(Å)	$2\theta_{101}$	$2\theta_{200}$	$2\theta_{110}$	d_{101}(Å)	d_{200}(Å)	d_{110}(Å)	D (nm)
Reference (ZnS)	3.777	6.188	30.897	28.833	48.148	2.8918	3.0940	1.8885	……
ZnS	4.702	6.179	31.019	28.860	……..	2.8795	3.0899	……..	13.15
$Zn_{0.9}Cd_{0.1}S$	4.645	6.264	31.407	28.462	……..	2.8448	3.1322	……..	15.19
$Zn_{0.8}Cd_{0.2}S$	4.810	6.333	30.306	28.146	……..	2.9456	3.1666	……..	19.82
$Zn_{0.5}Cd_{0.5}S$	4.016	6.488	……	27.461	45.088	…….	3.2440	2.0083	20.80
$Zn_{0.4}Cd_{0.6}S$	3.993	6.465	……	27.558	45.361	…….	3.2328	1.9969	23.30
Reference $Zn_{1-x}Cd_xS$	4.042	6.588	28.776	27.081	44.833	2.0200	3.2900	3.1000	……

3.5 Microscopic Studies

Electron microscopy were used to study the morphology of the synthesized nanostructures.

3.5.1 SEM Morphology Analysis

SEM images of the obtained ZnS and $Zn_{1-x}Cd_xS$ ternary sulfides nanostructures are shown in the **Figure 3.7 (a-e).** In the low magnification SEM image of ZnS, the nanostructure appears in much agglomerated form, with in a cluster of about 2.5 µm, without any significant impurity. However, with incorporation of little amount of Cd in $Zn_xCd_{1-x}S$ ternary sulfides when (X = 0.2) the agglomeration decreases and thus the cluster size also decreases upto 1.5 µm. Similarly as the Cd content increases in $Zn_xCd_{1-x}S$ ternary sulfides, the self-assembling decreases and nanostructure become well dispersed as it is clearly observed from the respective SEM images.

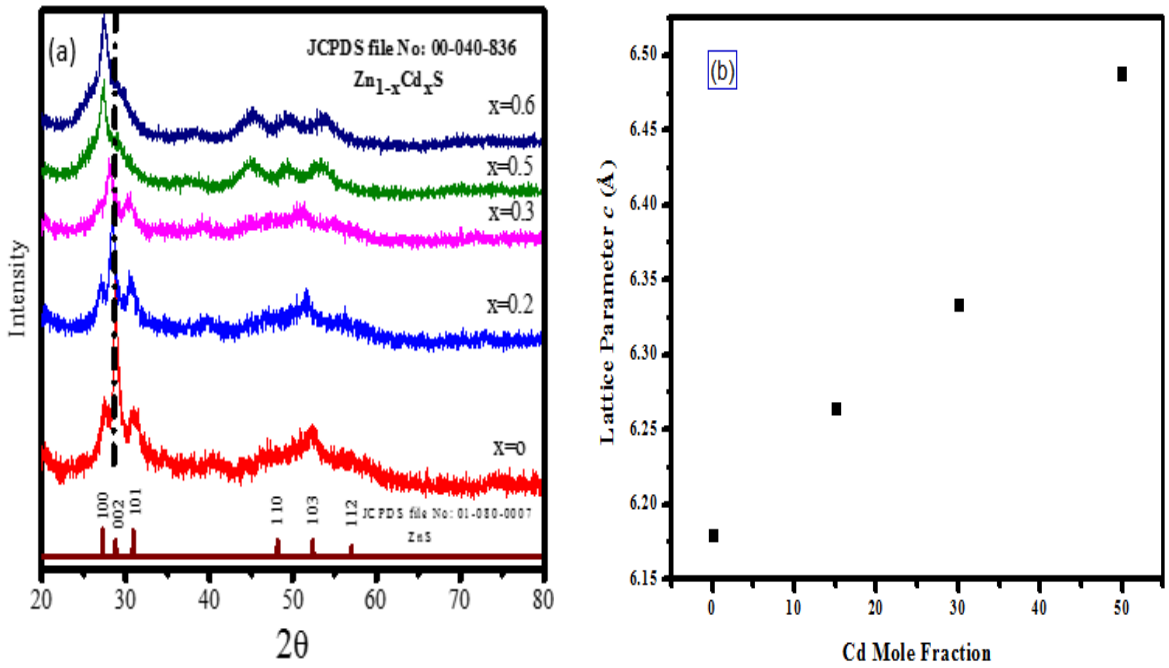

Figure 3.6 (a) PXRD Patterns of ZnS and $Zn_{1-x}Cd_xS$ ternary sulfides, (b) A linear relationship of lattice parameter c of $Zn_{1-x}Cd_xS$ as a function of Cd mole fraction, measured from XRD patterns.

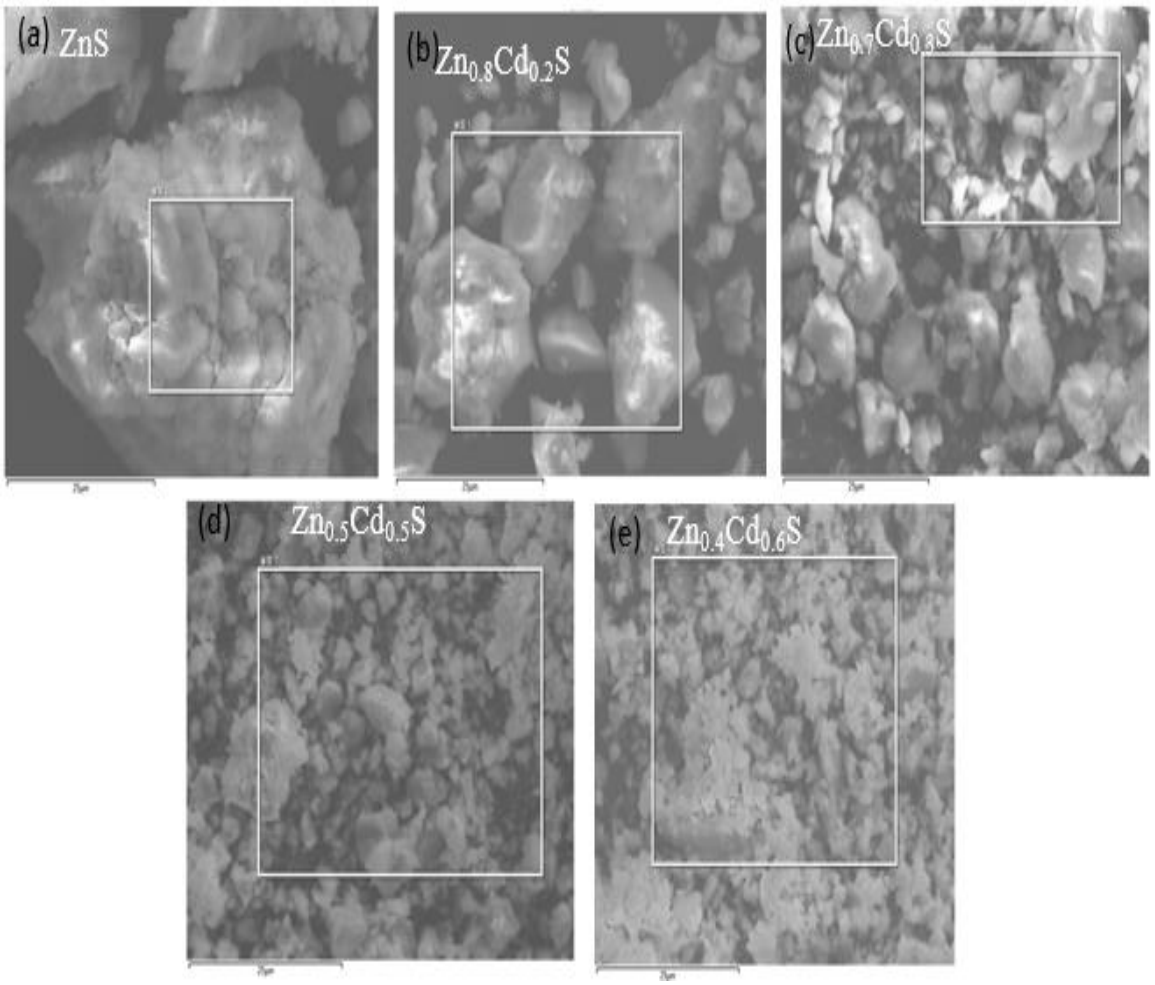

Figure 3.7 (a) SEM image of ZnS, (b) $Zn_{0.8}Cd_{0.2}S$, (c) $Zn_{0.7}Cd_{0.3}S$, (d) $Zn_{0.5}Cd_{0.5}S$ and (e) $Zn_{0.4}Cd_{0.6}S$ nanostructures.

3.5.2 TEM Morphology Analysis

TEM images of the pure ZnS and $Zn_{1-x}Cd_xS$ ternary sulfides nanostructure are depicted in **Figure 3.8 (a) and (b, c, d and e**) respectively. TEM image of ZnS and $Zn_{1-x}Cd_xS$ with little amount of Cd content (X = 0.2) reveal the nanostructure in more agglomerated form with layered and sheet like morphologies and their size range about 13 to 15 nm as calculated from PXRD. However in $Zn_{1-x}Cd_xS$ ternary sulfides nanostructure as the Cd content increases i.e. (X = 0.3, 0.5 and 0.6) gradually rod shape morphologies has been observed as can be seen in their respective TEM images. The reason for the composition based morphology transition could be as follows. A solid solution of $Zn_{1-x}Cd_xS$ nanostructured would be formed during the thermolysis processes, and the growth of the nanostructure

would involve competition between ZnS like (sphere or sheet) and the CdS like (rod) growth modes. Therefore, the Zn/Cd molar ratio in the reactant mixture influence the growth process and results in different morphologies of the formed $Zn_{1-x}Cd_xS$ nanostructures.

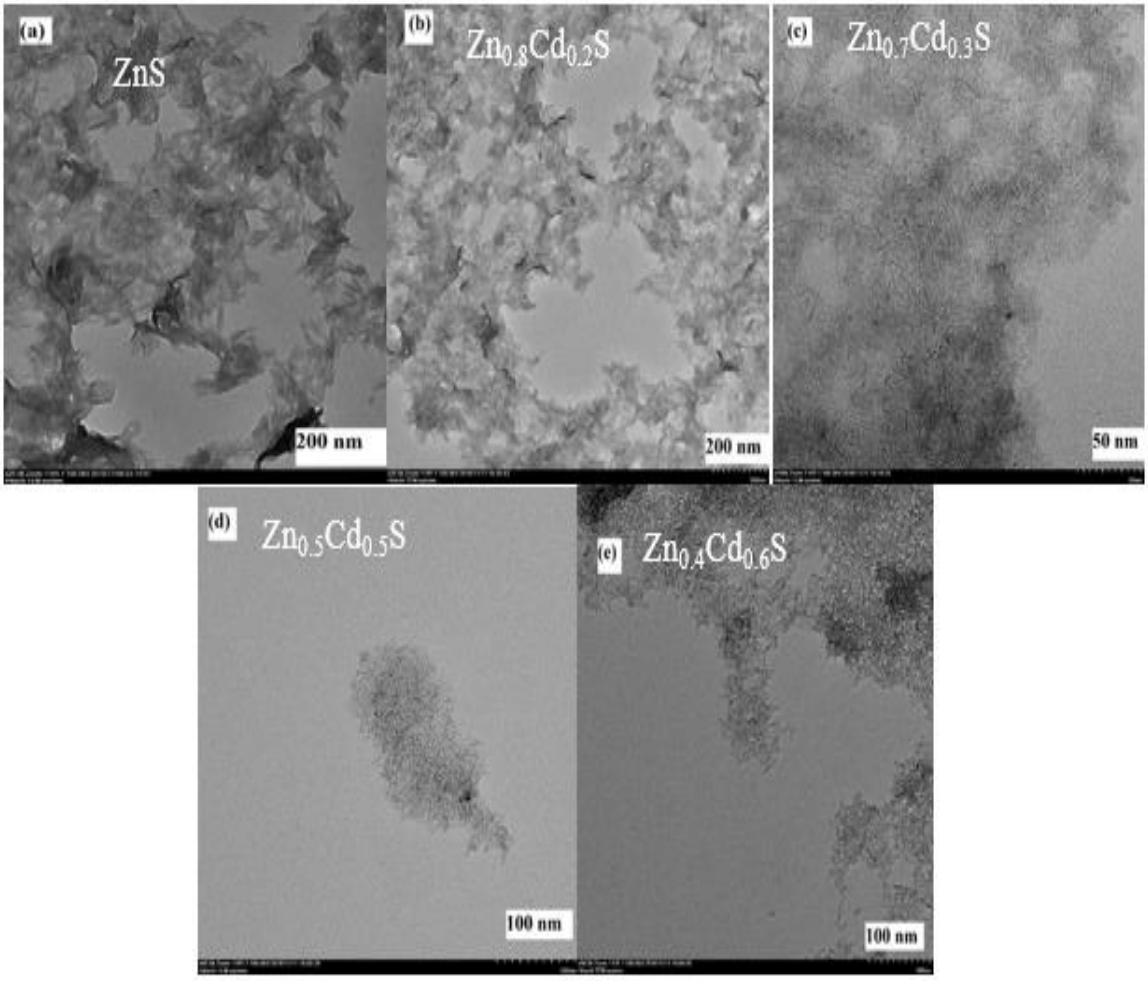

Figure 3.8 (a) TEM image of ZnS, (b) $Zn_{0.8}Cd_{0.2}S$, (c) $Zn_{0.7}Cd_{0.3}S$, (d) $Zn_{0.5}Cd_{0.5}S$ and (e) $Zn_{0.6}Cd_{0.4}S$ nanostructures

3.6 Energy Dispersive X-ray Spectroscopy

Energy dispersive X-ray spectroscopy were used to confirm elemental composition and purity of the synthesized nanostructures. **Figure 3.9 (a-e)** shows the EDS spectra of the synthesized ZnS and $Zn_{1-x}Cd_xS$ ternary sulfides nanostructure. The EDS spectrum of ZnS in **Figure 3.7 (a)** reveals the presence of Zn and S peaks confirming the formation of ZnS. The average atomic ratio of Zn:S is 46.7:40. **Figure 3.9(b)** shows the EDS spectrum Zn_{1-}

$_xCd_xS$ with lower Cd content (X = 0.2) which shows the presence of Zn, S as well as Cd peaks confirming the formation the formation $Zn_{1-x}Cd_xS$ ternary sulfides nanostructure. The average atomic ratio of Zn:S:Cd is 31.4:39.2:8.2. Similarly **Figure 3.9 (c, d and e)** depict the EDS spectra of $Zn_{1-x}Cd_xS$ with higher concentrations (X = 0.3, 0.5 and 0.6) which shows the presence of Zn, S and Cd peaks once again confirming the formation of $Zn_{1-x}Cd_xS$ ternary sulfides nanostructure respectively. The presence of oxygen peaks in each spectrum reveals oxygen atom in the nanostructures which may attributed to the distilled water used during synthesis. **Table 3.3** shows the composition of synthesized ZnS and Cd doped ZnS respectively in atomic as well as mass percentage ratio.

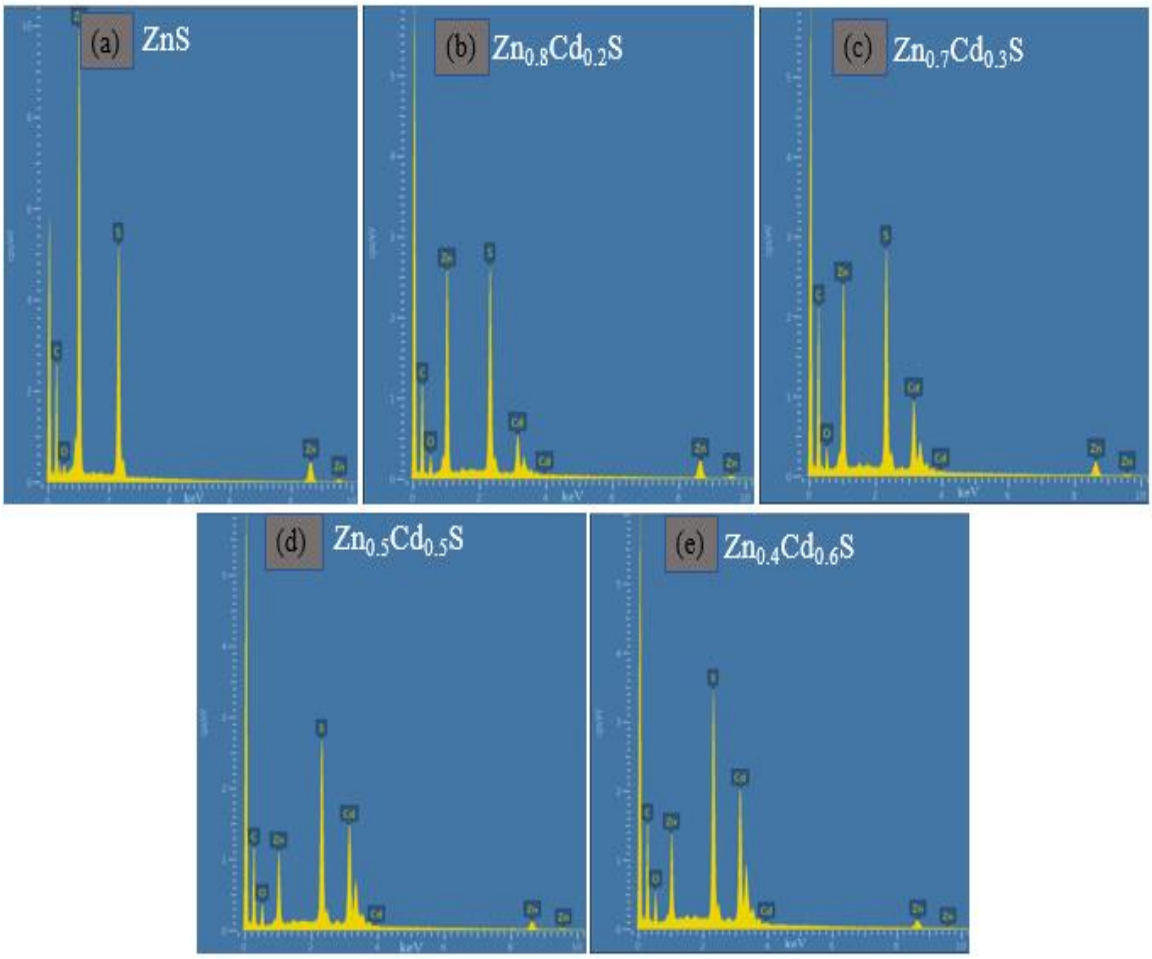

Figure 3.9 (a) EDS spectrum of ZnS, (b) $Zn_{0.8}Cd_{0.2}S$, (c) $Zn_{0.7}Cd_{0.3}S$, (d) $Zn_{0.5}Cd_{0.5}S$ and (e) $Zn_{0.6}Cd_{0.4}S$ nanostructures.

Table 3.3 Elemental Composition of $Zn_xCd_{1-x}S$ where (X= 0.0, 0.2, 0.3, 0.5, and 0.6) for a .b .c, d, and e respectively Obtained from EDS Analysis

(a)			
Element	**(k eV)**	**Mass %**	**Atomic %**
O K	0.526	3.19	9.2
S K	2.307	30.59	44.0
Zn K	8.63	66.21	46.7
(b)			
Element	**(k eV)**	**Mass %**	**Atomic %**
O K	0.526	7.41	21.2
S K	2.307	27.49	39.2
Zn K	8.63	44.91	31.4
Cd L	3.132	20.16	8.2
(c)			
Element	**(k eV)**	**Mass %**	**Atomic %**
O K	0.526	8.08	21.2
S K	2.307	25.39	36.5
Zn K	8.63	38.20	27.4
Cd L	3.132	28.76	12.4
(d)			
Element	**(k eV)**	**Mass %**	**Atomic %**
O K	0.526	10.91	32.5
S K	2.307	22.35	33.2
Zn K	8.63	19.76	14.4
Cd L	3.132	47.223	19.9
(e)			
Element	**(k eV)**	**Mass %**	**Atomic %**
O K	0.526	11.50	34.2
S K	2.307	21.44	31.8
Zn K	8.63	18.42	13.4
Cd L	3.132	48.70	20.6

3.7 Photocatalytic Activity

The optical study shows that the synthesized nanostructures have band gap which can response in the visible region and thus these nanostructures can act as photocatalyst in the visible region. To confirm the spectral response of these nanostructures, photocatalytic activity for photodegradation of methylene blue aqueous solution was performed in the presence of synthesized nanostructures under the direct sunlight at constant magnetic stirring.

3.7.1 Photocatalytic Degradation of Methylene Blue (MB)

Methylene blue is brown powder cationic dye which gives blue color by forming its aqueous solution showing maximum absorbance around 664 nm. It is most commonly used for coloring paper, temporary hair colorant, dyeing cotton wools etc. It is well-known that the dye industry has a problem of removal of methylene blue (MB) because of its high solubility in water. Although methylene blue is not considered to be a more toxic dye but it can leads to severe problems like diarrhea, vomiting, difficulties in breathing and nausea after inhalation in living organism and similarly like other dyes it can disturb ecosystem if present higher concentration in the water [10,11, 12]. Due to this reason, methylene blue was selected to be degraded photocatalytically using synthesized nanostructured $Zn_{1-x}Cd_xS$ as photocatalyst.

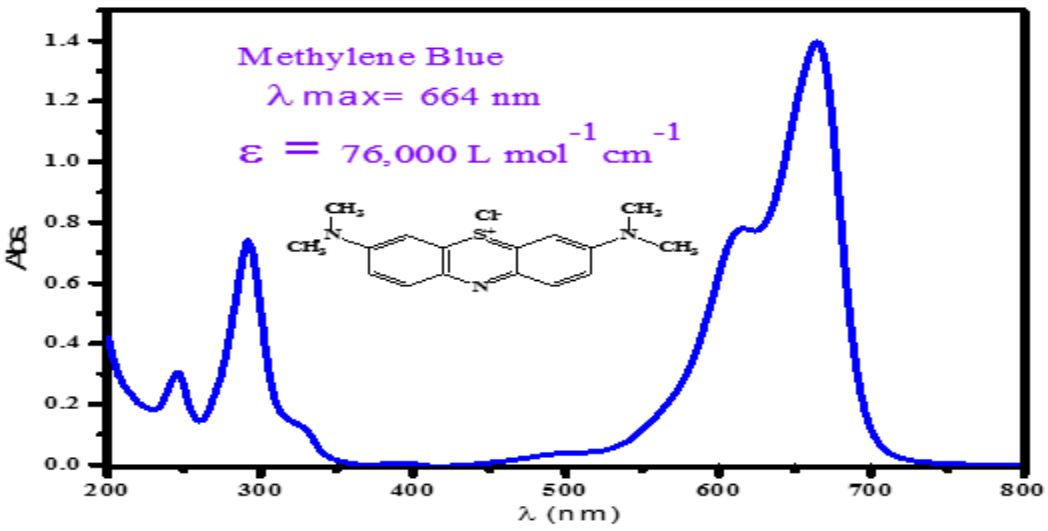

Figure 3.10 Structure and UV-Vis Spectrum of Methylene Blue

3.7.2 Mechanism of Photocatalytic Degradation of Dyes

$Zn_{1-x}Cd_xS$ semiconductor nanostructure have attracted much more interest now a days because of their unique photochemical and photophysical properties to treat dyes waste water [13, 14]. Mechanistically the photocatalytic reaction of $Zn_{1-x}Cd_xS$ like other photoresposive semiconductors, is initiated when an electron is excited from its valence band to conduction band as a result of absorption relevant light irradiation with energy ($h\nu$) equal to or greater than the band gap energy of $Zn_{1-x}Cd_xS$ which leads to electron hole pair generation**.(Eq. 3**).The photogenerated hole reacts with water to generate hydroxyl radical (OH•) **(Eq.4)** which is an efficient oxidizer for organic materials, attack on adsorb or nearby dye molecules to the catalyst surface, thereby degrading it to final product. The electrons in the conduction band react with molecular oxygen and get converted into superoxide radical anion **(Eq.5)** which yield hydrogen peroxide upon protonation **(Eq.6).** The hydrogen peroxide further dissociates into hydroxyl radical which again accelerates the photodegradation process **(Eq.7 and Eq. 8).**

$$Zn_{1-x}Cd_xS + h\upsilon \rightarrow Zn_{1-x}Cd_xS\{e^-(CB) + h^+(VB)\} \quad (\mathbf{3.4})$$

$$H_2O + h^+ \rightarrow \dot{OH} + H^+ \quad \mathbf{(3.5)}$$

$$O_2 + e^- \rightarrow O_2^{\cdot} \quad \mathbf{(3.6)}$$

$$O_2^{\cdot} + 2H^+ \rightarrow H_2O_2 \quad \mathbf{(3.7)}$$

$$H_2O_2 \rightarrow \dot{HO} + \dot{HO} \quad \mathbf{(3.8)}$$

$$\dot{OH} + Dye \rightarrow degradation\ products \quad \mathbf{(3.9)}$$

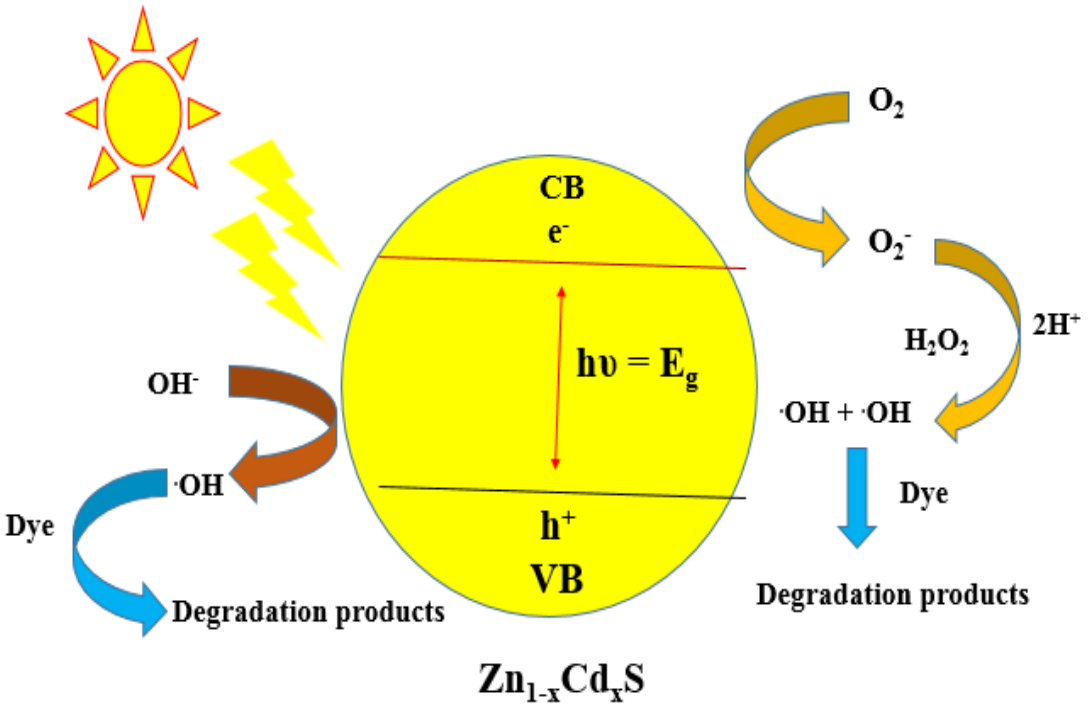

Figure 3.11 Proposed mechanism for Photodegradation of methylene blue using $Zn_{1-x}Cd_xS$ ternary sulfides nanostructure as a photocatalyst

In this work the photocatalytic performance of zinc cadmium ternary sulfide $Zn_{1-x}Cd_xS$ (where X= 0.0, 0.2, 0.3, 0.5, 0.6) was evaluated for the degradation of MB dye under direct sunlight. The degradation progress of the methylene blue was monitored by observing decrease in the intensity of absorption bands at 664 nm as a function of irradiation time. The UV-Visible spectral changes in the concentration of methylene blue aqueous solution with reaction time in the presence of $Zn_{1-x}Cd_xS$ ternary sulfides nanostructure as a photocatalyst, is displayed in Figure3(a—e), respectively. In the presence of $Zn_{1-x}Cd_xS$ nanostructure with higher Cd content (X= 0.5 and 0.6) 99.4 % and 100 % decolorization of the dye was achieved in 120 minutes respectively (Fig. 3.12 d and e).

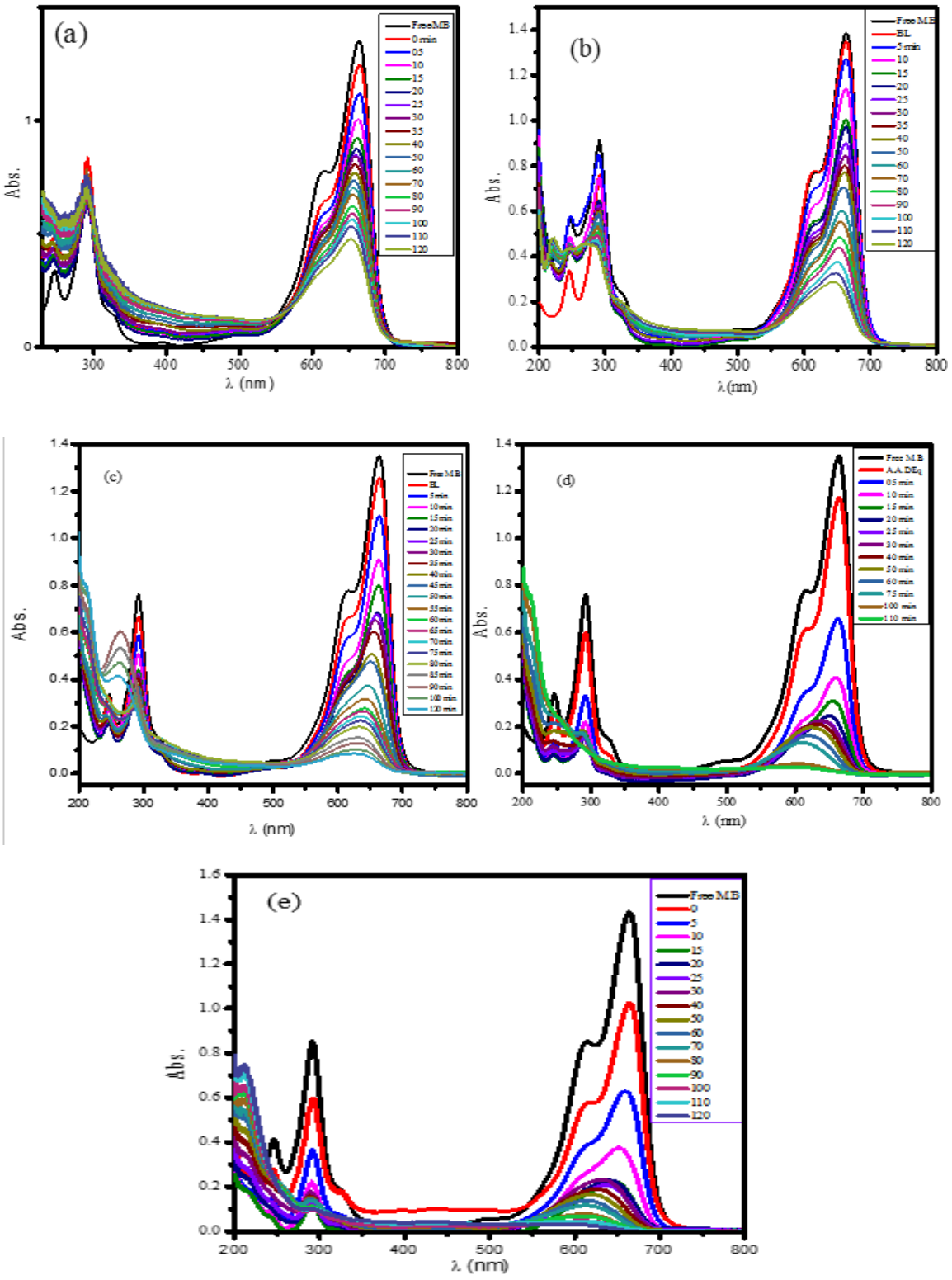

Figure 3.12 UV-Visible spectral changes of Methylene Blue solution with reaction time in the presences of $Zn_{1-x}Cd_xS$ as photocatalyst under sunlight (where X= 0.0, 0.2, 0.3, 0.5, and 0.6) for a—e respectively.

The photocatalytic behavior of the synthesized nanostructure was confirmed with $Zn_{0.4}Cd_{0.6}S$ nanostructures by the fact that doing the same reaction in the dark. Only 15 % and 20 % decrease in the absorbance was observed for the 60 and 120 minutes which is due to adsorption of dye on the surface of nanostructure and furthermore no significant increase in adsorption or degradation was observed till 180 minutes.

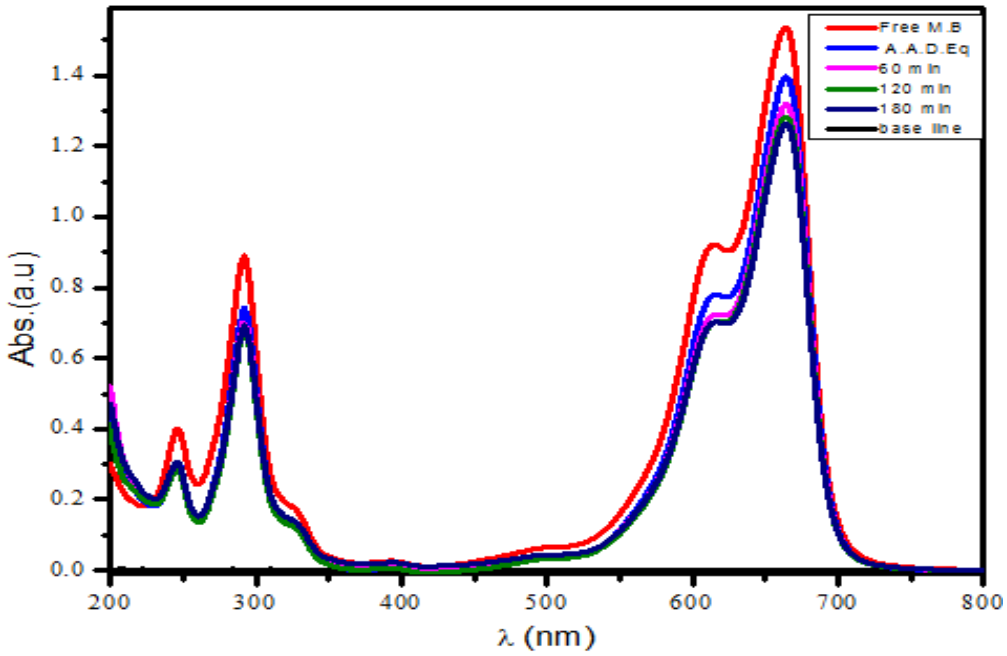

Figure 3.13 Methylene Blue with $Zn_{0.4}Cd_{0.6}S$ nanostructures in dark

The degradation efficiency of the synthesized nanostructures in term of percent degradation was calculated using equation (2.1) and higher degradation rate was observed for $Zn_{1-x}Cd_xS$ nanostructure with higher Cd content (X= 0.5 and 0.6). Their comparative degradation rates are shown in the figure 3.14. The higher degration rate observed in $Zn_{1-x}Cd_xS$ nanostructure with higher Cd content may be attributed to these nanostructures due to two possible reasons, (a) higher absorption capacity covering UV-Visible range of solar irradiation because of narrower band gap relative to ZnS, (b) high photocatalytic efficiency due slow rate of charge carrier's recombination relative to the pure CdS [15].

The rate constant (k) of the degradation reaction was calculated by using equation 2.2. The degradation reaction follows pseudo first order kinetics, as a linear relation exists between the dye concentration and irradiation time (Fig. 3.15). The measured k values for the degradation reaction by $Zn_{1-x}Cd_xS$ with x = 0.0, 0.2, 0.3, 0.5 and 0.6 was 0.0076 min^{-1},

0.0143 min^{-1}, 0.0304 min^{-1}, 0.0425 min^{-1}, 0.0430 min^{-1} respectively. From the study of kinetics of photodegradation once again confirmed that rate of reaction increases continuously with increase in Cd content in $Zn_{1-x}Cd_xS$ nanostructure and the reasons may be the same mentioned above.

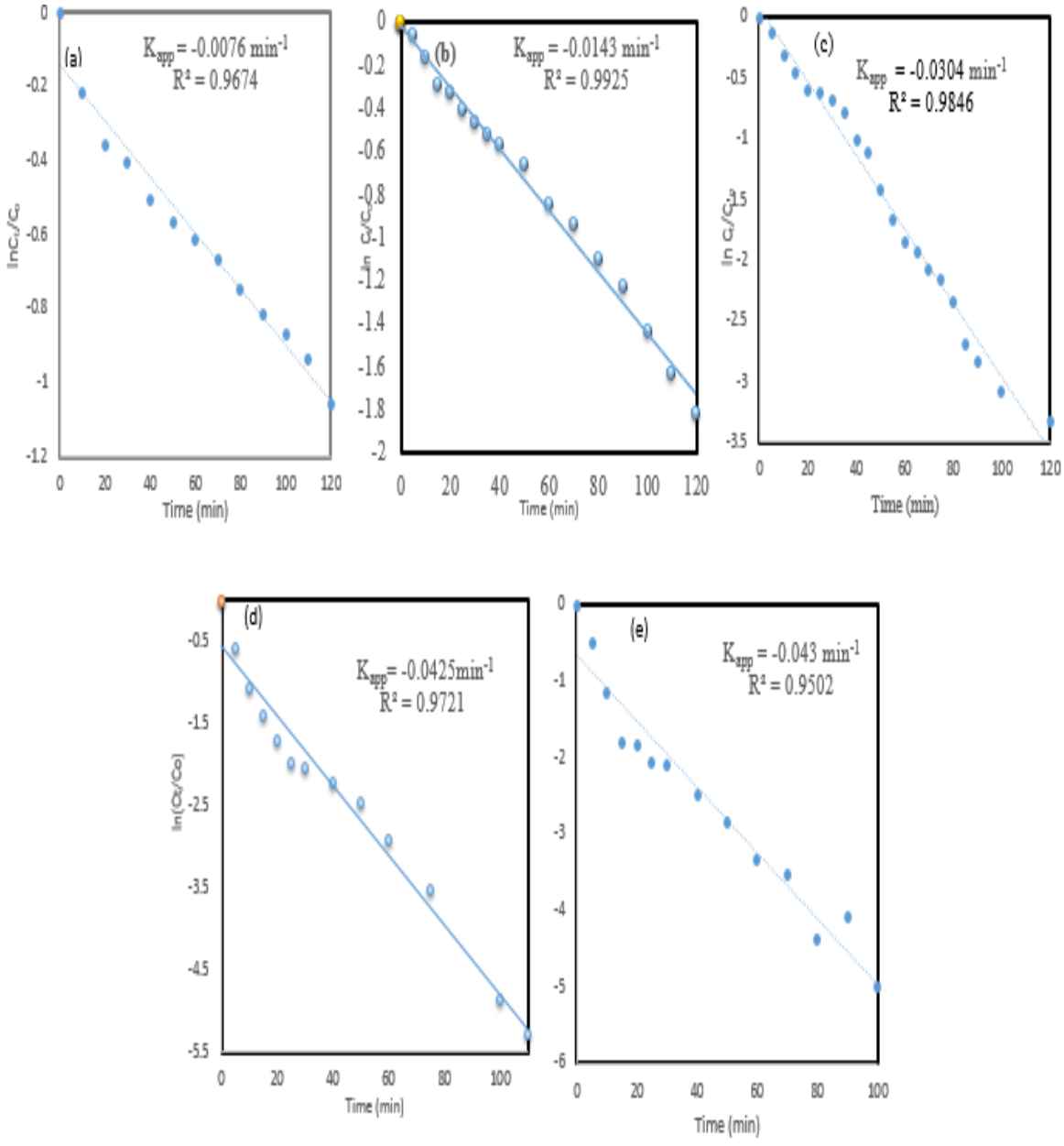

Figure 3.15 The degradation kinetics of Methylene Blue as a function of irradiation time in the presence of synthesized nanostructure $Zn_{1-x}Cd_xS$ nanostructure Photocatalyst (Where X= 0.0, 0.2, 0.3, 0.5 and 0.6 for a, b, c, d and e respectively)

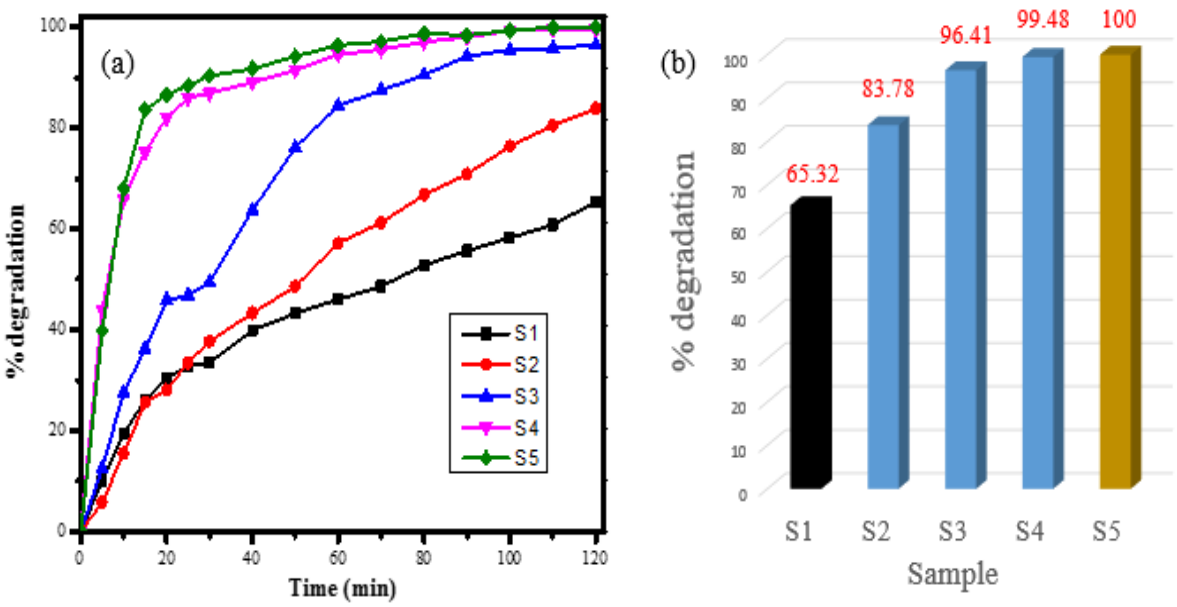

Figure 3.14 (a) % degradation of Methylene Blue with $Zn_{1-x}Cd_xS$ nanostructure photocatalyst as function of Time (minutes), (b) % degradation of M.B dye with $Zn_{1-x}Cd_xS$ nanostructure after 120 minutes. (Where X= 0.0, 0.2, 0.3, 0.5 and 0.6 for S1, S2, S3, S4 and S5 respectively)

Conclusion

ZnS and $Zn_{1-x}Cd_xS$ nanostructures of hexagonal phase were successfully synthesized using a new strategy, via thermal decomposition of self-prepared single source precursor (zinc cadmium bisdimethydithiocarbamate) $Zn_{1-x}Cd_x$-$(DMDTC)_2$ by simple reflux method at 120 ^oC. PXRD, UV-Vis DRS, SEM, TEM and EDS analysis were used to characterize the synthesized nanostructures. Optical (UV-Vis DRS) and structural (PXRD) investigation showed that incorporation of cadmium content in nanostructures have significant effect on the properties zinc sulfide. The absorption peak progressively red shifted with increasing cadmium content which consequently reduce the band gap from 3.4 eV (ZnS) to 2.5 eV for $Zn_{1-x}Cd_xS$ nanostructures with higher content of cadmium (x=0.6). The crystallite size of the as synthesized nanostructure calculated from PXRD data was 12-20 nm and increase in d-spacing was observed with incorporation of cadmium. SEM images shows decrease in clusters formation while TEM images displays appearance of rod shape morphology with increase in cadmium content. EDS spectra confirm the presence of zinc, cadmium and sulfur approximately in the same ratio, in which they were mixed to synthesize the materials. The photoresponse of the synthesized nanostructures were investigated for photodegradation of methylene blue dye and highest activity was observed for $Zn_{1-x}Cd_xS$ having higher cadmium content (x=0.6). The composition modulated optical properties of $Zn_{1-x}Cd_xS$ nanostructure may lead to the development of materials for photocatalyst and optoelectronic devices. It can be expected that this simple, cheap and mild method can be extended to synthesize some other important semiconducting, ternary and even quaternary metal sulfide nanomaterials with tunable composition, morphology and size just by using corresponding mixed-metal dimethyldithiocarbamate as a superior single source precursor.

References

1. Zia-ur-Rehman; Ibrahim, S.; Khan, A.; Imran, M.; Naseer, M. M.; Khan, I.; Shah, A.; Tahir, M. N.; Muneeb-ur-Rahman; Awan, I. Z., Homobimetallic zinc (II) dithiocarbamates: synthesis, characterization and in vivo antihyperglycemic activity. *J. Coord. Chem.*, **2016,** *69*, 551-561.
2. Serpone, N.; Lawless, D.; Khairutdinov, R., Size effects on the photophysical properties of colloidal anatase TiO2 particles-size quantization or direct transitions in this indirect semiconductor. *J. Phys. Chem.* **1995,** *99*, 16646-16654.
3. Sadhu, S.; Patra, A., Lattice Strain Controls the Carrier Relaxation Dynamics in $Cd_xZn_{1-x}S$ Alloy Quantum Dots. *J. Phys. Chem. C.*, **2012,** *116*, 15167-15173.
4. Selvaraj, R.; Qi, K.; Pandian, S. B. S.; Meetani, M. A.; Al Wahaibi, B.; Al Lawati, H.; Al Kindy, S. M.; Kim, Y.; Sillanpää, M., Morphology-Controlled Synthesis of $Cd_xZn_{1-x}S$ Solid Solutions: An Efficient Solar Light Active Photocatalyst for the Degradation of 2, 4, 6-Trichlorophenol. *J. Environ. Prot.*, **2016,** *7*, 1605.
5. Xing, C.; Zhang, Y.; Yan, W.; Guo, L., Band structure-controlled solid solution of $Cd_xZn_{1-x}S$ photocatalyst for hydrogen production by water splitting. *Int. J. Hydrogen Energy* **2006,** *31*, 2018-2024.
6. Zu, S.; Wang, Z.; Liu, B.; Fan, X.; Qian, G., Synthesis of nano-$Cd_xZn_{1-x}S$ by precipitate-hydrothermal method and its photocatalytic activities. *J. Alloys Compd.* **2009,** *476*, 689-692.
7. Zhang, W.; Zhong, Z.; Wang, Y.; Xu, R., Doped Solid Solution: $(Zn_{0.95}Cu_{0.05})_{1-x}Cd_xS$ Nanocrystals with High Activity for H2 Evolution from Aqueous Solutions under Visible Light. *J. Phys. Chem.C* **2008,** *112*, 17635-17642.
8. Wang, W.; Germanenko, I.; El-Shall, M. S., Room-Temperature Synthesis and Characterization of Nanocrystalline CdS, ZnS, and $Cd_xZn_{1-x}S$. *Chem. Mater.* **2002,** *14*, 3028-3033.
9. Wang, D.-H.; Jia, L.; Wu, X.-L.; Lu, L.-Q.; Xu, A.-W., One-step hydrothermal synthesis of N-doped TiO_2/C nanocomposites with high visible light photocatalytic activity. *Nanoscale* **2012,** *4*, 576-584.

10. Soltani, N.; Saion, E.; Hussein, M. Z.; Erfani, M.; Abedini, A.; Bahmanrokh, G.; Navasery, M.; Vaziri, P., Visible light-induced degradation of methylene blue in the presence of photocatalytic ZnS and CdS nanoparticles. *Int. j. mol. Sci.* **2012,** *13*, 12242-12258.
11. Cao, Y. C.; Wang, J., One-pot synthesis of high-quality zinc-blende CdS nanocrystals. *J. Amer. Chem. Soc.* **2004,** *126*, 14336-14337.
12. Pirkanniemi, K.; Sillanpää, M., Heterogeneous water phase catalysis as an environmental application: a review. *Chem. Sphere.* **2002,** *48*, 1047-1060.
13. Sharma, P.; Rana, D.; Umar, A.; Kumar, R.; Chauhan, M.; Chauhan, S., Synthesis of cadmium sulfide nanosheets for smart photocatalytic and sensing applications. *Ceram. Int.* **2016,** *42*, 6601-6609.
14. Fard, N. E.; Fazaeli, R.; Ghiasi, R., Band gap energies and photocatalytic properties of CdS and Ag/CdS nanoparticles for azo dye degradation. *Chem. Eng. Technol.* **2016,** *39*, 149-157.
15. Garaje, S. N.; Apte, S. K.; Naik, S. D.; Ambekar, J. D.; Sonawane, R. S.; Kulkarni, M. V.; Vinu, A.; Kale, B. B., Template-Free Synthesis of Nanostructured $Cd_xZn_{1-x}S$ with Tunable Band Structure for H_2 Production and Organic Dye Degradation Using Solar Light. *Environ. Sci. technol.* **2013,** *47*, 6664-6672.